Ancient Mitogenomes Reveal the Evolutionary History and Biogeography of Sloths

Frédéric Delsuc, Melanie Kuch, Gillian C. Gibb, Emil Karpinski, Dirk Hackenberger, Paul Szpak, Jorge G. Martínez, Jim I. Mead, H. Gregory Gregory Mcdonald, Ross D. E. Macphee, et al.

Ancient Mitogenomes Reveal the Evolutionary History and Biogeography of Sloths

Frédéric Delsuc,[1,13,*], Melanie Kuch,[2] Gillian C. Gibb,[1,3], Emil Karpinski,[2,4] Dirk Hackenberger,[2] Paul Szpak,[5] Jorge G. Martínez,[6] Jim I. Mead,[7,8] H. Gregory McDonald,[9] Ross D. E. MacPhee,[10] Guillaume Billet,[11] Lionel Hautier,[1,12] and Hendrik N. Poinar[2,*]

Author list footnotes

[1]Institut des Sciences de l'Evolution de Montpellier (ISEM), CNRS, IRD, EPHE, Université de Montpellier, Place Eugène Bataillon, 34095 Montpellier Cedex 5, France

[2]McMaster Ancient DNA Centre, Department of Anthropology, McMaster University, 1280 Main Street West, Hamilton, ON L8S 4L8, Canada

[3]Wildlife and Ecology Group, School of Agriculture and Environment, Massey University, Centennial Drive, Hokowhitu, Palmerston North 4410, New Zealand

[4]Department of Biology, McMaster University, 1280 Main Street West, Hamilton, ON L8S 4L8, Canada

[5]Department of Anthropology, Trent University, 1600 West Bank Drive, Peterborough, ON K9L 0G2, Canada

[6]Instituto Superior de Estudios Sociales, CONICET-Instituto de Arqueología y Museo, Universidad Nacional de Tucumán, San Martín 1545, CP4000 San Miguel de Tucumán, Argentina

[7]The Mammoth Site, Hot Springs, Hot Springs, SD 57747, United States of America

[8]East Tennessee State University Natural History Museum, 1212 Suncrest Drive, Johnson City, TN 37615, United States of America

[9]Bureau of Land Management, Utah State Office, 440 West 200 South #500, Salt Lake City, UT 84101, United States of America

[10]Division of Vertebrate Zoology/Mammalogy, American Museum of Natural History, Central Park West & 79th Street, New York, NY 10024, United States of America

[11]Centre de Recherche en Paléontologie - Paris (CR2P), UMR CNRS 7207, Sorbonne Université, Muséum National d'Histoire Naturelle, 57 Rue Cuvier, 75005 Paris, France

[12]Mammal Section, Life Sciences, Vertebrate Division, The Natural History Museum, Cromwell Road, South Kensington, London SW7 5BD, United Kingdom

[13]Lead contact

[*]**Correspondence:** frederic.delsuc@umontpellier.fr (F.D.), poinarh@mcmaster.ca (H.N.P.)

Keywords

Ancient DNA; Mitogenomics; Phylogenetics; Molecular dating; Extinct sloths; Morphology; Convergence; Biogeography; GAARlandia.

GRAPHICAL ABSTRACT

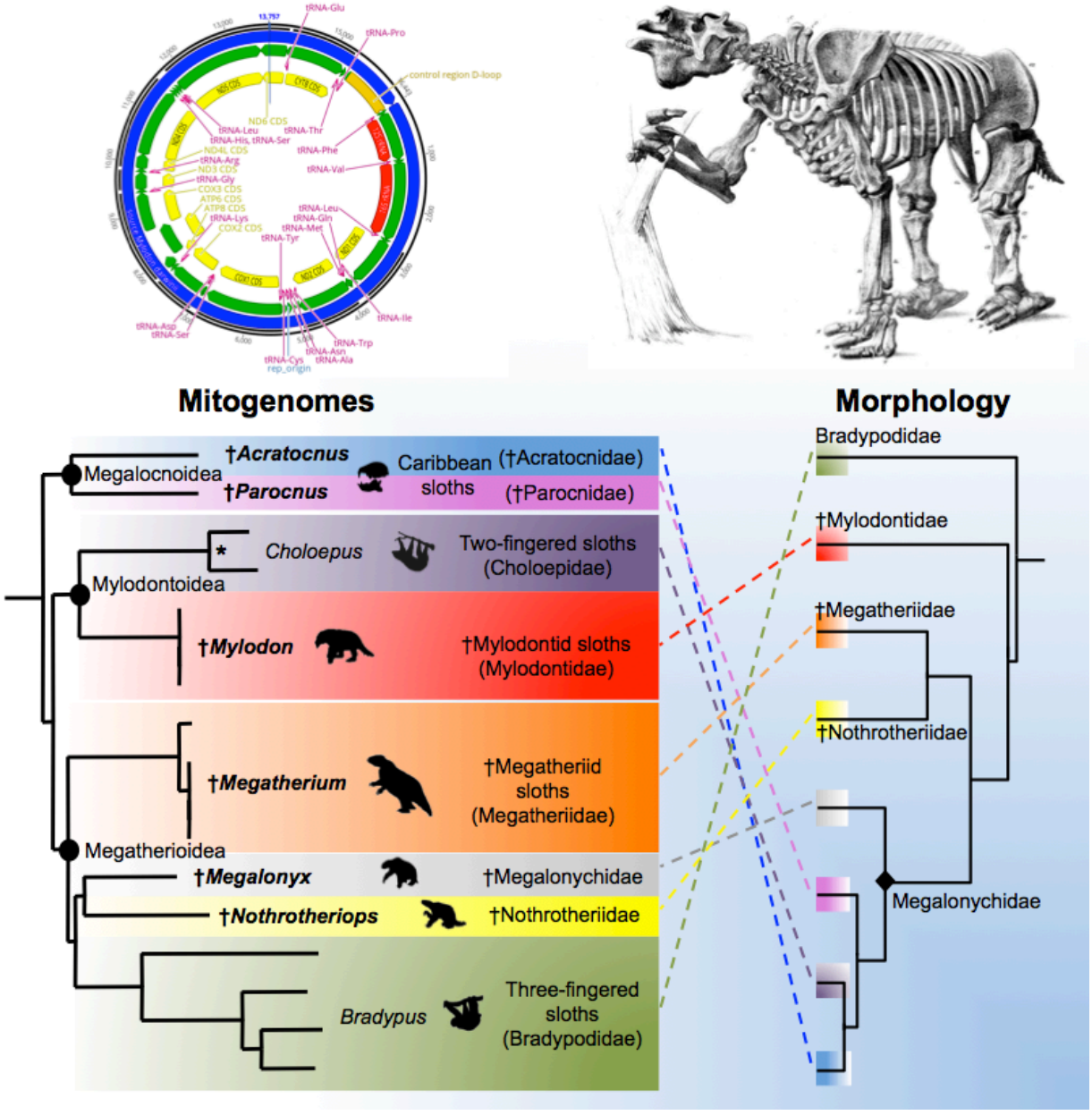

SUMMARY

Living sloths represent two distinct lineages of small-sized mammals that independently evolved arboreality from terrestrial ancestors. The six extant species are the survivors of an evolutionary radiation marked by the extinction of large terrestrial forms at the end of the Quaternary. Until now sloth evolutionary history has mainly been reconstructed from phylogenetic analyses of morphological characters. Here we used ancient DNA methods to successfully sequence 10 extinct sloth mitogenomes encompassing all major lineages. This includes the iconic continental ground sloths *Megatherium*, *Megalonyx*, *Mylodon*, and *Nothrotheriops*, and the smaller endemic Caribbean sloths *Parocnus* and *Acratocnus*. Phylogenetic analyses identify eight distinct lineages grouped in three well-supported clades and whose interrelationships are markedly incongruent with the currently accepted morphological topology. We show that recently extinct Caribbean sloths have a single origin but comprise two highly divergent lineages that are not directly related to living two-fingered sloths, which instead group with *Mylodon*. Moreover, living three-fingered sloths do not represent the sister-group to all other sloths but are nested within a clade of extinct ground sloths including *Megatherium*, *Megalonyx*, and *Nothrotheriops*. Molecular dating also reveals that the eight newly recognized sloth families all originated between 36 and 28 million years ago (Mya). The early divergence of recently extinct Caribbean sloths around 35 Mya is consistent with the debated GAARlandia hypothesis postulating the existence at that time of a biogeographic connection between northern South America and the Greater Antilles. This new molecular phylogeny has major implications for reinterpreting sloth morphological evolution, biogeography, and diversification history.

INTRODUCTION

Sloths (Xenarthra; Folivora) are represented today by six living species, distributed in tropical forests throughout the Neotropics and conventionally placed in two genera: *Choloepus*, the two-fingered sloths (two species), and *Bradypus,* the three-fingered sloths (four species). Tree sloths typically weigh 4-8 kg and are strictly arboreal. However, the living species represent only a small fraction of the past Cenozoic diversity of sloths. More than 100 genera of sloths have been systematically described, including the large-bodied species of the Pliocene and Pleistocene popularly known as ground sloths of the Ice Age. This includes the giant ground sloth (*Megatherium americanum*) with an estimated body mass of more than 4000 kg, and Darwin's ground sloth (*Mylodon darwinii*), named for Charles Darwin who collected its first fossil remains. Like their closest xenarthran relatives (anteaters and armadillos), sloths originated in South America and successfully invaded Central and North America prior to the completion of the Isthmus of Panama [1]. Pleistocene North American representative taxa include the Shasta ground sloth (*Nothrotheriops shastensis*) and Jefferson's ground sloth (*Megalonyx jeffersonii*) whose range extended up to Alaska. Late Quaternary ground sloths went extinct ~10,000 years before present (yrbp) as part of the megafaunal extinction that occurred at the end of the latest glaciation [2]. However, sloths also reached a number of Caribbean islands, giving rise to an endemic radiation best known from Quaternary taxa (*Megalocnus*, *Neocnus*, *Acratocnus*, and *Parocnus*) [3] that became extinct only shortly after the appearance of humans in the Greater Antilles ~4,400 yrbp [4]. When and how sloths colonized the West Indies is still disputed. The oldest accepted fossil evidence dates from the Early Miocene of Cuba [5], although discoveries in Puerto Rico [6,7] demonstrate that terrestrial mammal possibly including sloths, were already in the Greater Antilles by the Early Oligocene. These findings would be consistent with the debated GAARlandia (GAAR: Greater Antilles + Aves Ridge) paleobiogeographic hypothesis

postulating the existence of a land bridge via the Aves Ridge that would have briefly emerged between 35 and 33 Mya and connected northern South America to the Greater Antilles [6].

Until recently, the phylogenetic relationships of sloths were almost exclusively investigated from analyses of morphological data. Cladistic analyses using maximum parsimony [8–11] and Bayesian reconstructions [12] based predominantly on craniodental characters have consistently recovered topologies defining five major sloth lineages, currently recognized as families. In these phylogenetic reconstructions, modern three-fingered sloths always appear as the sister-group of all other sloths and are considered to have retained a number of ancestral characters [8]. Extant two-fingered sloths are also consistently found close to or nested within Caribbean sloths as the sister-group of either *Acratocnus* [3] or *Neocnus* [8,12] and are classified within Megalonychidae, together with other extinct sloths related to *Megalonyx*. It is noteworthy, however, that there is currently no fossil that could be convincingly assigned to the two independent lineages that led to extant tree sloths [13]

The vast majority of Quaternary sloth taxa became extinct so recently that numerous remains in the form of bones, teeth, fragments of skin with hair and osteoderms, claws with their keratinous sheaths, and paleofeces are still well preserved. The amount of subfossil material available makes sloths an ideal group to leverage the power of ancient DNA to decipher their radiation. In a pioneering study, Höss et al. [14] tested 45 samples from diverse sloth taxa, but only two specimens of Darwin's ground sloth (*Mylodon darwinii*) from Mylodon Cave (Chile) yielded short mitochondrial ribosomal gene fragments. Recently, a bone from the same cave with high endogenous DNA content allowed assembly of a high-quality complete mitogenome for *Mylodon darwinii* using shotgun sequencing [15]. Exceptional preservation of paleofecal material of the extinct Shasta ground sloth (*Nothrotheriops shastensis*) from Gypsum Cave (Nevada) enabled characterization of its diet by ancient DNA barcoding of plant remains [16,17]. Paleofeces from this cave also yielded short PCR-amplified mitochondrial [18] and nuclear [19]

sequences allowing investigation of the phylogenetic affinities among extinct and extant sloths. Nowadays, DNA capture-based targeted enrichment is emerging as the method of choice in ancient DNA studies. It has recently been used to reconstruct partial mitogenomes for *Nothrotheriops shastensis* and *Mylodon darwinii* [20]. Moreover, it has been demonstrated that baits designed from ancestral sequences reconstructed from extant xenarthran mitogenomes can improve capture success from species for which there is no closely related extant taxa such as the extinct glyptodont *Doedicurus* [21].

Both molecular [14,15,18–20] and morphological [8,9,12] phylogenetic studies have supported the diphyletic origin of the two living sloth genera implying an independent evolution of arboreality from terrestrial ancestors. However, molecular studies are actually in conflict with morphological inferences regarding the precise phylogenetic positions of extant sloths in strongly supporting a close relationship between *Choloepus* and *Mylodon* [14,15,18,20] and firmly grouping *Bradypus* with *Nothrotheriops* [18–20]. In order to understand the causes of this incongruence, we used ancient DNA techniques to sequence the mitogenomes of 10 extinct Quaternary sloths. Phylogenetic analyses of these new mitogenomic data support a topology that is markedly incongruent with the currently accepted morphological framework. Our results have major implications for interpreting sloth morphological evolution and should stimulate a complete rethinking of our current understanding of the evolutionary history of this group.

RESULTS

Ten new ancient sloth mitogenomes

Using capture baits designed from ancestral sequences inferred using available xenarthran mitogenomes [21], we successfully captured, sequenced, and assembled nearly complete

mitogenomes for 10 ancient sloth samples representing the six extinct genera *Mylodon*, *Megatherium*, *Megalonyx*, *Nothrotheriops*, *Parocnus*, and *Acratocnus*, and encompassing all major late Quaternary sloth lineages (Table 1). Radiocarbon dates for these samples ranged between 10,395 ± 40 radiocarbon years before present (^{14}C yrbp) for *Acratocnus ye* and 45,800 ± 2000 ^{14}C yrbp for *Megalonyx jeffersonii*. Samples stemmed from diverse locations including temperate and tropical regions of the continental Americas and the Greater Antilles, and from different sources with osteological material and paleofeces. For five of the 10 samples, de novo assembly of captured reads reconstructed a single contig covering the targeted mitogenome. To ensure that our results were reproducible between experiments, we attempted capture using the ancestrally designed baits on a *Mylodon darwinii* sample (Lib67) and succeeded in replicating the identical mitogenome previously assembled from the same sample, but via shotgun sequencing [15]. Moreover, mitogenomes from three different paleofecal samples, attributed to an undetermined Megatheriinae from Peñas de las Trampas (Argentina) dated between 19,610-12,510 ^{14}C yrbp [22,23] yielded nearly identical sequences (99.9% identity). The mitogenomes from these three samples were 97% identical to one obtained from a bone of the extinct giant ground sloth *Megatherium americanum*. This level of mitochondrial sequence divergence typically falls within the intraspecific diversity of extant sloths [24] and implies that these paleofeces likely came from *Megatherium americanum*.

To assess the authenticity of our ancient sloth mitogenomes, we examined the fragment length distributions and the presence of DNA damage in all mapped reads. As expected, reads were short (Table 1) and showed expected DNA damage patterns (Figure 1). Damage patterns differed between osteological material and paleofeces, with osteological samples showing higher levels of DNA damage with up to 41% cytosine deamination on the oldest bone sample, *Megalonyx jeffersonii* (45,800 ^{14}C yrbp). Our youngest Caribbean sloth samples from the Republic of Haiti also showed substantial levels of deamination (up to 33% for *Acratocnus ye*

and up to 35% for *Parocnus serus*). The mapped reads from the three *Megatherium americanum* paleofecal samples from Peñas de las Trampas in the extremely arid Argentinean Puna, and the paleofeces of the Shasta ground sloth (*Nothrotheriops shastensis*) from Rampart cave exhibited the lowest levels of post-mortem damage (up to only 7% for *Megatherium americanum* Lib_X18) and the highest average read lengths (Table 1). However, this seemingly better preservation may be due the Uracil-DNA glycosylase and Endonuclease VIII treatment used during library preparation from paleofeces [25]. The well-preserved *Mylodon darwinii* bone found in Mylodon cave showed an intermediate level of DNA damage (up to 15%). In contrast, the *Mylodon darwinii* osteoderm sample from the same cave presented a higher DNA damage pattern similar to other osteological samples (up to 36%). Such patterns of post-mortem mutations and short read lengths typical of ancient DNA molecules support the endogenous origin of the reads captured from our ancient samples.

Mitogenomic phylogeny of living and extinct sloths

Phylogenetic analyses of our dataset using both maximum likelihood and Bayesian approaches resulted in a topology that was markedly incongruent with the morphological tree (Figure 2). The molecular phylogeny identified eight major lineages belonging to three strongly supported clades, with interrelationships (Figure 2A) that are in strong conflict with morphological analyses (Figure 2B). In particular, the family Megalonychidae as currently conceived was polyphyletic, with three independent origins recovered for its constitutive members (extinct Jefferson's ground sloth *Megalonyx jeffersonii*, extinct Caribbean sloths, and extant two-fingered sloths). While the Caribbean sloth group was unambiguously monophyletic (BP_{RAxML} = 100 / $BP_{IQ\text{-}TREE}$ = 100 / $PP_{MrBayes}$ = 1.0 / $PP_{PhyloBayes}$ = 1.0), *Parocnus serus* and *Acratocnus ye* nevertheless belonged to two deeply divergent lineages. However, this Caribbean clade was not closely related to modern two-fingered sloths, nor to Jefferson's ground sloth, which is in sharp contrast to morphological

inferences (Figure 2B). In fact, Caribbean sloths appeared to represent the sister-group to all other sloths, even though this position remained statistically uncertain (BP_{RAxML} = 30 / $BP_{IQ\text{-}TREE}$ = 41 / $PP_{MrBayes}$ = 0.68). Extant two-fingered sloths (*Choloepus* spp.) were closely related to extinct Darwin's ground sloth (*Mylodon darwinii*) with strong statistical support from all methods (BP_{RAxML} = 98 / $BP_{IQ\text{-}TREE}$ = 100 / $PP_{MrBayes}$ = 1.0 / $PP_{PhyloBayes}$ = 1.0). Most phylogenetic reconstruction methods also supported the grouping of Jefferson's ground sloth (*Megalonyx jeffersonii*) with the Shasta ground sloth (*Nothrotheriops shastensis*) (BP_{RAxML} = 74 / $BP_{IQ\text{-}TREE}$ = 78 / $PP_{MrBayes}$ = 1.0). These two extinct lineages were the sister-group of modern three-fingered sloths (*Bradypus* spp.) with good support (BP_{RAxML} = 75 / $BP_{IQ\text{-}TREE}$ = 89 / $PP_{MrBayes}$ = 1.0 / $PP_{PhyloBayes}$ = 1.0). Three-fingered sloths thus did not represent the sister-group of all other sloth species as had been concluded by morphological studies (Figure 2B). Instead, they were firmly nested within a strongly supported clade composed of the extinct giant ground sloth *Megatherium* together with *Megalonyx* and *Nothrotheriops* (BP_{RAxML} = 85 / $BP_{IQ\text{-}TREE}$ = 94 / $PP_{MrBayes}$ = 1.0 / $PP_{PhyloBayes}$ = 1.0).

Molecular dating of the sloth radiation

The molecular chronogram obtained under the autocorrelated lognormal (LN) relaxed clock model (Figure 3A) revealed an ancient origin of the eight newly identified sloth lineages. Their rapid diversification occurred in a narrow time window of less than 10 million years (Myr), in the Late Eocene / Early Oligocene, between approximately 36 and 28 Mya. The two earliest divergences within the sloth radiation almost perfectly coincided with the Eocene / Oligocene boundary (33.9 Mya). The early emergence of Caribbean sloths (Node 1) was estimated at 35 ± 5 Mya and the separation of the two other major clades of sloths (Node 4) at 34 ± 5 Mya. The ancient monophyletic origin of Caribbean sloths was compatible with the GAARlandia

hypothesis (35-33 Mya). The ancient divergence between the two Caribbean sloths (Node 2) was estimated to 29 ± 5 Mya. Within the second major sloth clade (Node 3), modern two-fingered sloths (*Choloepus* spp.) and the extinct Darwin's ground sloth (*Mylodon darwinii*) also diverged 29 ± 5 Mya. Within the third major sloth clade (Node 5), the extinct giant ground sloth (*Megatherium americanum*) split from the other three lineages at 31 ± 5 Mya, modern three-fingered sloths diverged from the extinct Jefferson's ground sloth (*Megalonyx jeffersonii*) and Shasta ground sloth (*Nothrotheriops shastensis*) at 29 ± 5 Mya (Node 7), which in turn separated at 28 ± 5 Mya (Node 6). Posterior density distributions of mean divergence times illustrated the synchronicity of many divergences among the eight sloth lineages (Figure 3B). Very similar distributions centering on the Early to Late Oligocene transition at 29 Mya were obtained for the divergences between *Parocnus* and *Acratocnus* (Node 2), *Choloepus* and *Mylodon* (Node 3), and *Bradypus* versus *Megalonyx* + *Nothrotheriops* (Node 7). Similarly, the age distributions of the two earliest splits (Nodes 1 and 4) were centered on the Eocene / Oligocene boundary and contemporaneous with the proposed GAARlandia land bridge.

Reconstruction of the ancestral sloth dental formula

The sloth dentition in most taxa shows a morpho-functional distinction between an anteriorly located caniniform and the molariforms that form the tooth row (Figure 4A). In order to reinterpret dental character evolution on a sloth phylogeny including most available fossils, we used our newly inferred molecular topology as a backbone in maximum likelihood and parsimony reconstructions of ancestral character states performed on the morphological matrix of Varela et al. [12]. Both methodologies retrieved consistent results, but reconstructions of the sloth ancestral dental formula differed depending on whether the molecular backbone was enforced or not (Figure 4B). All reconstructions proposed an ancestral dental formula of five

upper and four lower teeth for sloths, in association with the absence of diastema, and the caniniform shape of the anterior most teeth (Figure 4; characters 2(0), 6(0), 19(1), and 21(0)). The main differences involved the size of the upper (Cf) and lower (cf) caniniforms. When considering the topology of the unconstrained morphological analyses, the reduced condition of the caniniforms (characters 13(0) and 14(0)) was reconstructed as ancestral, while reconstructions using a molecularly constrained topology retrieved large caniniforms (characters 13(1) and 14(1)) as the ancestral state.

DISCUSSION

A revised phylogeny and taxonomy for living and extinct sloths

Our mitogenomic tree revisits the phylogenetic relationships among living and extinct sloths compared to the currently accepted morphological picture. Mitochondrial genomes have limitations as phylogenetic markers with cases of mito-nuclear discordance resulting from ancient hybridization events reported in mammals [26,27]. The relatively short internal branches might also reflect the occurrence of incomplete lineage sorting. However, a parallel study of sloth phylogeny based on ancient nuclear collagen proteins independently corroborates our mitogenomic results [28]. The high congruence observed between the mitochondrial and nuclear genome results provides substantial evidence for the newly proposed sloth phylogeny.

Based on this extensively revised phylogeny and reevaluated timescale, we propose a new taxonomic framework for sloths (Folivora), in which the eight molecularly identified lineages are recognized as distinct families (Figure 2A). Some of these molecular lineages correspond to traditional families: Bradypodidae, Mylodontidae, Megatheriidae, and Nothrotheriidae. However, Megalonychidae as classically defined is polyphyletic and should be divided into distinct

families. We propose that the family Megalonychidae be restricted to genus *Megalonyx* and meaningfully related genera, and to classify extant two-fingered sloths of the genus *Choloepus* in the monotypic family Choloepodidae. As the two distinct lineages of Caribbean sloths diverged at about the same time as the other newly defined families, we propose respectively elevating the Acratocnini and Parocnini tribes [3] to family level into Acratocnidae and Parocnidae. Finally, we recommend reorganizing sloth superfamily names and content so that they correspond to the three strongly supported main clades recovered in all our analyses (Figures 2A): Megalocnoidea (Acratocnidae and Parocnidae), Mylodontoidea (Mylodontidae and Choloepidae), and Megatherioidea (Megatheriidae, Megalonychidae, Nothrotheriidae, and Bradypodidae). This newly proposed taxonomic framework would hopefully be adopted in systematic paleontological studies to reassess the numerous Cenozoic fossil taxa for which molecular data are inaccessible. Such a reassessment is needed to make sense of the rich sloth fossil record in light of available molecular data.

Reinterpreting sloth evolution in light of the new molecular phylogeny

The new molecular results are in strong conflict with cladistic [3,8,10,29] and Bayesian [12] analyses of morphological characters (Figure 2). However, in the details, analyses of morphological characters provide only limited statistical support for most proposed suprafamilial relationships. Gaudin [8] recognized that alternative hypotheses respectively placing *Bradypus* with Megatheriidae and *Choloepus* with Mylodontidae, as suggested by early molecular studies [14,18] and confirmed by our analyses, could not be statistically rejected. The Bayesian analysis of Varela et al. [12] also provides a tenuous phylogenetic signal as indicated by the large proportion of nodes receiving posterior probability < 0.95. These observations illustrate the

limited power of existing morphological matrices for resolving higher-level phylogenetic relationships within sloths.

Such an apparently high level of incongruence between morphology and molecules is reminiscent of the case of placental mammals until molecular studies [30] revealed an unsuspected high level of morphological homoplasy [31]. Our new molecular phylogenetic framework likewise suggests that numerous morphological characters used to reconstruct sloth interfamilial relationships must have evolved convergently. The most striking example of morphological convergence in sloths concerns Megalonychidae. The molecular evidence demonstrates that, as currently defined, Megalonychidae is polyphyletic, with three independent origins for the lineages represented by *Megalonyx*, *Choloepus*, and the Caribbean sloths. Yet the monophyly of this clade has been consistently retrieved in morphological studies [3,8,10,12]. Gaudin [8], for example, recovered 20 unequivocal synapomorphies supporting Megalonychidae, most of which were related to features of the trenchant caniniforms (Figure 4). The strength of this argument depends on the validity of the assumption that tooth row structure as seen in *Bradypus* is ancestral, while that of *Choloepus* is derived, which was ultimately influenced by the early branching position of *Bradypus* on the sloth morphological phylogeny [8]. The dental formula of extinct and extant sloths is surprisingly conservative, as it never exceeds five upper and four lower teeth (Figure 4). However, the homology between the upper and lower caniniforms in *Choloepus* and *Bradypus* has recently been reinterpreted based on developmental data. Hautier et al. [32] showed that the dental pattern of *Bradypus* might represent a neotenic condition with the retention of a deciduous caniniform and the absence of a functional caniniform in adults. They suggested that a large permanent caniniform as observed in *Choloepus* could represent the ancestral condition for sloths. Our ancestral reconstruction under the molecular constraint indicating large caniniforms as the most likely ancestral state for sloths is in line with this developmental scenario, as well as with the presence of a large

caniniform in *Pseudoglyptodon*, considered to be the earliest fossil sloth [33]. This finding that dental homologies have been misinterpreted between the two living sloth genera mitigates the potential weight of dental features related to the size and shape of the caniniforms in phylogenetic and systematic studies. In all cases, the utmost caution should be used when coding dental features that are prone to functional convergence.

An unexpected outcome of our molecular investigation is that the endemic Caribbean sloths are not closely related to extant two-fingered sloths of the genus *Choloepus*, but instead represent one of the three main clades of the sloth radiation. This is a radical departure from the prevailing morphological consensus that has prevailed for decades [3,10,34]. Gaudin [8], however, also noted that *Choloepus* shares a number of craniodental characters with Mylodontidae that he interpreted as convergences. In light of our results confirming the close relationship between *Choloepus* and *Mylodon* revealed by previous molecular studies [14,15,18,20], these characters might in fact constitute true synapomorphies for this clade as originally intuited in pre-cladistic studies of comparative anatomy [35,36]. Moreover, our results challenge the position of living three-fingered sloths of the genus *Bradypus* as the sister-group to all other sloths retrieved in most morphological studies [8–10,12]. Instead, we found strong support for *Bradypus* being nested within a clade of extinct ground sloths, including the Shasta ground sloth *Nothrotheriops* as proposed by previous molecular studies [18–20], but also the giant ground sloth *Megatherium americanum*, and Jefferson's ground sloth *Megalonyx jeffersonii* (Figure 2A). Here also Gaudin [8] noticed a number of seemingly convergent morphological features between *Bradypus* and Megatheriidae, which ought to be re-evaluated as signatures of common ancestry as suggested by early anatomical studies [35–37].

A new timescale for sloth evolution and biogeography

Our molecular dating results unveil a rapid diversification at the base of the sloth radiation with an almost synchronous origin of the three main clades at the Eocene / Oligocene boundary ~35 Mya followed by the divergence of all eight major lineages in a narrow time window framing the Early Oligocene between 31 and 28 Mya (Figure 3). This time period corresponds to a global glacial maximum characterized by the formation of the Antarctic ice sheet and the set up of the circum-Antarctic oceanic current following the abrupt decrease in terrestrial temperature at the Eocene-Oligocene transition [38]. In South America, this prompted the transition from humid tropical forest environments to drier and more open habitats [39]. According to our molecular estimates these environmental changes might have triggered the diversification of sloth families among other mammalian herbivore communities. The fossil record nevertheless implies at most an Early Miocene origin for most sloth families [40]. Our results favor a long-fuse model of sloth diversification, with molecular estimates of interfamilial divergences predating their paleontological origin by more than 10 Myr. This model invites a reconsideration of the taxonomic status of Oligocene sloth fossils with uncertain relationships, such as *Orophodon*, *Octodontotherium*, and *Deseadognathus,* in light of the apparent antiquity of the newly defined families.

Unsurprisingly, given the major differences between morphological and molecular topologies, our mitogenomic timescale markedly contrasts with the one recently obtained by Varela et al. [12] using a Bayesian morphological clock model combined with tip-dating. This directly affects the timing of the origins of the two living sloth lineages given their revised phylogenetic positions. With regard to three-fingered sloths, their divergence from all other sloths was estimated at ~40 Mya with morphological data [12], whereas our estimate places the separation of *Bradypus* from its relatives *Nothrotheriops* and *Megalonyx* at ~29 Mya (Figure 3). However, the most notable inconsistency between morphological and molecular estimates

concerns the timing of the Caribbean sloth radiation, formerly thought to include extant two-fingered sloths (*Choloepus*) based on morphological data. The morphological clock results place the divergence between *Acratocnus* and *Parocnus* at only ~8 Mya and the divergence between *Parocnus* and *Choloepus* at ~5 Mya [12]. In striking contrast, our molecular timescale indicates that the two monophyletic Caribbean sloth genera diverged ~29 Mya, which is almost identical to our dating of the separation of *Choloepus* and *Mylodon* (Figure 3). So ancient a divergence between the species *Acratocnus ye* and *Parocnus serus*, both endemic to Hispaniola [3], implies an early diversification of insular sloths within the West Indies. The megalocnoids subsequently diversified (Figure 5), likely in part through island-island vicariance as the land masses comprising present day Cuba-Hispaniola-Puerto Rico drifted apart in the Miocene [41]. The early fossil record for the diversification of Caribbean sloths is, however, very limited. A partial femur of uncertain affinities found in the Early Oligocene of Puerto Rico was tentatively attributed to “Megalonychidae” (species A in Figure 5; [6]). The only other non-Quaternary fossil is *Imagocnus zazae* from the Early Miocene of Cuba, which has clear folivoran affinities (Figure 5; [42]). Given the deep divergence between Parocnidae and Acratocnidae, it is likely that other ancient sloth fossils remain to be found in the Greater Antilles. Overall, our molecular dating results show that recent Quaternary extinctions wiped out six of the eight newly identified sloth families that originated in the Early Oligocene more than 28 Mya, including two ancient endemic Caribbean sloth lineages.

From the biogeographical point of view, the rapid radiation of the three major sloth lineages, including the Caribbean clade, is consistent with a single colonization of the Caribbean islands taking place around 35 Mya. This estimation would be compatible with the debated GAARlandia hypothesis, which postulates the brief existence 33-35 Mya of a land bridge that subaerially united northernmost South America and the Greater Antilles-Aves Rise magmatic arc [6,41] (Figure 5). This landspan is thought to correspond to the uplift of the Aves Ridge, a paleo-island

arc that is now submerged in the Caribbean Sea, west of the current Lesser Antilles. As originally conceived, the GAARlandia hypothesis was based on mammal distributions, and attempted to explain how several South American groups might have managed to reach the islands without invoking overwater dispersal. More recently, molecular phylogenies obtained for other terrestrial Caribbean mammals have mostly rejected the hypothesis, because the origin of the investigated taxon was either too ancient in the case of solenodontids [43,44] or too recent for capromyid [45] and sigmodontine [46] rodents, and primates [47]. Sloths are thus the first Caribbean mammalian group for which molecular dating based on mitogenomics provides support for GAARlandia. The dispersal of other terrestrial Caribbean taxa may have been enabled by this temporary dispersal corridor, including a genus of toads [48] and three different groups of spiders [49–51]. The existence of this dispersal corridor would also explain the presence of caviomorph rodent fossils of South American origin in the Greater Antilles by the Early Oligocene [7].

Overall, our new molecular phylogenetic framework and timescale tell a story of sloth evolution very different from that of the one previously told by morphology alone. Our results have important implications for reinterpreting many aspects of sloth evolution that have been previously based on the morphological phylogenetic picture such as morpho-functional adaptations [9], body size evolution [52,53], and macroevolutionary patterns [12]. We hope our study will stimulate a complete rethinking of the evolutionary history of sloths with reassessment of morphological characters in light of the significant amount of convergence revealed by the new molecular framework.

ACKNOWLEDGMENTS

We thank Suzanne Jiquel, Marie-Dominique Wandhammer, Andrew Currant, Régis Debruyne, Adolfo F. Gil, Alex D. Greenwood, Svante Pääbo, François Pujos, Rodolpho Salas Gismondi, and David Steadman for access to sloth specimens, John Southon for radiocarbon dating, Philippe Münch, Pierre-Henri Fabre, Fabien Condamine, Laurent Marivaux, and Pierre-Olivier Antoine for discussions on the biogeographical context, Rémi Allio for his help with ggridges, and Renaud Lebrun for access to the MRI microCT facilities. This work was supported by grants from the Centre National de la Recherche Scientifique (CNRS), the Scientific Council of the Université de Montpellier (UM), the Investissements d'Avenir managed by Agence Nationale de la Recherche (CEBA, ANR-10-LABX-25-01; CEMEB, ANR-10-LABX-0004), Agence Nationale de la Recherche (GAARAnti, ANR-17-CE31-0009), the Natural Sciences and Engineering Research Council of Canada (NSERC, no. RGPIN04184-15) and the Canada Research Chairs programme. This is contribution ISEM 2019-092-SUD of the Institut des Sciences de l'Evolution de Montpellier.

AUTHOR CONTRIBUTIONS

Conceptualization: F.D., H.N.P.; Data curation: M.K., E.K., H.N.P.; Formal analysis: F.D., L.H., G.B.; Funding acquisition: F.D., L.H., H.N.P.; Investigation: M.K., G.C.G., E.K., D.H., P.S., H.N.P.; Resources: F.D., J.G.M., J.I.M., H.G.M., R.D.E.M., H.N.P.; Supervision: F.D., H.N.P.; Validation: F.D., H.N.P.; Visualization: F.D., L.H.; Writing – original draft: F.D., L.H.; Writing – review & editing: F.D., M.K., G.C.G., E.K., J.G.M., H.G.M., R.D.E.M., G.B., L.H., H.N.P.

DECLARATION OF INTERESTS

The authors declare no competing interests.

FIGURE LEGENDS

Figure 1. DNA damage profiles of mapped mitochondrial reads for the 10 different libraries. The fragment misincorporation plots represent the frequency of cytosine deamination per position at both strands of mapped sequence reads (5' C=>T and 3' G=>A).

Figure 2. Mitogenomic versus morphological phylogenies of living and extinct sloths. (A) Maximum likelihood phylogram obtained with RAxML under the best partition model for sloth mitogenomes. Values at nodes represent maximum-likelihood bootstrap percentages under the best partition model using RAxML (BP_{RAxML}) and IQ-TREE ($BP_{IQ\text{-}TREE}$), and clade posterior probabilities under the best partition model using MrBayes ($PP_{MrBayes}$) and the CAT-GTR mixture model using PhyloBayes ($PP_{PhyloBayes}$). An asterisk (*) indicates strong support from all statistical indices (BP ≥ 95 and PP ≥ 0.99) whereas a dash (-) indicates that the node was not recovered with the corresponding method. Taxa in bold are those sequenced in this study. Colors highlight the eight newly proposed families and bullets (●) the three new superfamilies. Complete phylograms are available as Figures S1-S4. See also Tables S1-S3. (B) Time-calibrated phylogenetic relationships among the main sloth lineages as reconstructed from morphological data showing the five currently recognized families: Bradypodidae (limited to the extant three-fingered sloths in the genus *Bradypus*), Mylodontidae (extinct sloths related to *Mylodon*), Megatheriidae (extinct sloths related to *Megatherium*), Nothrotheriidae (extinct sloths related to

447 *Nothrotheriops*), and Megalonychidae (including extinct sloths related to *Megalonyx*, extinct
448 Caribbean sloths, and extant two-fingered sloths of the genus *Choloepus*) (modified from [12]).
449 Dash lines highlight the incongruence between the molecular and the morphological topologies.
450 Silhouettes are from phylopic.org.

451

452 **Figure 3. Time-calibrated phylogeny of modern and ancient sloths based on complete**
453 **mitogenomes.** (A) Bayesian chronogram obtained using PhyloBayes under the CAT-GTR+G4
454 mixture model and the best-fitting autocorrelated lognormal (LN) relaxed molecular clock model.
455 Colors highlight the eight newly proposed families. The complete chronogram with 95%
456 credibility intervals is available as Figure S5. (B) Bayesian posterior density distributions of
457 divergence dates for the seven numbered nodes representing the diversification of the eight
458 newly recognized sloth families. The main geological periods follow the geological time scale of
459 the Geological Society of America (E, early; M, middle; L, late; Paleo., Paleocene; Pli., Pliocene;
460 P., Pleistocene). Silhouettes are from phylopic.org.

461

462 **Figure 4. Reinterpretation of dental evolution in sloths under the new phylogenetic**
463 **framework.** (A) 3D reconstructions of the skulls of a two-fingered sloth (*Choloepus didactylus*
464 UM 789N; left) and a three-fingered sloth (*Bradypus tridactylus* MZS 03557; right) showing the
465 six characters used for reconstructing the sloth ancestral dental features with states illustrated
466 following Varela et al. [12]: character #6, diastema [(0) absent or rudimentary; (1) elongate];
467 #13, size of upper caniniform (Cf) [(0) smallest tooth; (1) greatly enlarged; (2) neither the
468 smallest nor enlarged]; #14, size of lower caniniform (cf) [(0) smallest tooth; (1) greatly enlarged;
469 (2) neither the smallest nor enlarged]; #19, morphology of Cf/cf [(0) molariform; (2) caniniform;
470 (3) incisiform]; #21, position of Cf relative to the anterior edge of the maxilla [(0) right at the

edge; (1) near the edge; (2) well-separated from the anterior edge]; #23, fossa on palatal surface of maxilla posterior to Cf [(0) absent; (1) present]. (B) Schematic representations of the upper and lower tooth rows in *Choloepus* (left) and *Bradypus* (right), and maximum likelihood reconstructions of the sloth ancestral dental morphotype based respectively on the unconstrained (left) and constrained (right) ML topologies using a molecular backbone inferred from the morphological character matrix of Varela et al. [12].

Figure 5. Biogeographical context of the extinct Caribbean sloth radiation. Distribution of sloth fossil remains in the Greater and Lesser Antilles with recent Quaternary extinct species (†) and Tertiary fossils (*) (adapted from [3]). Species sequenced in this study are shown in bold. Species A corresponds to a small femur found in the Oligocene of Puerto Rico with uncertain sloth affinities [6]. The Aves Ridge is an ancient volcanic arc that is now entirely submerged in the Caribbean Sea. The dashed arrow indicates the hypothesized GAARlandia land bridge linking northern South America to the Greater Antilles around the Eocene-Oligocene transition (33-35 Mya) resulting from the uplift of the Aves Ridge at that time. Bathymetric map courtesy of NOAA National Centers for Environmental Information.

TABLE LEGEND

Table 1: Sample origins, radiocarbon dates, and mitogenome assembly statistics.

STAR * METHODS

- Key resources table
- Contact for resource sharing
- Experimental model and subject details
- Method details
- Data and software availability

CONTACT FOR RESOURCE SHARING

Further information and requests for resources should be directed to, and will be fulfilled by the lead contact author Frédéric Delsuc (Frederic.Delsuc@umontpellier.fr).

EXPERIMENTAL MODEL AND SUBJECT DETAILS

The 10 extinct sloth samples used in this study come from different specimen sources and are stored in natural history museums in Europe, USA, and Argentina (Table 1). For Darwin's ground sloth (*Mylodon darwinii*), we used two different samples both collected at Mylodon Cave (Última Esperanza, Chile) in the form of a bone (NHMUK PV M8758) stored at the Natural History Museum (London, UK) and a skin sample with osteoderms (MNHN 1905-4) stored at the Muséum National d'Histoire Naturelle (Paris, France). The *Mylodon* bone NHMUK PV M8758 was previously used to obtain a complete mitogenome using shotgun sequencing [15] of the same library as the one used here for sequence capture. For Jefferson's ground sloth (*Megalonyx jeffersonii*), we used a bone (PMA P98.6.28) collected at Big Bone Cave (TN, USA)

and conserved at the Academy of Natural Sciences of Drexel University (Philadelphia, PA, USA). For Shasta's ground sloth (*Nothrotheriops shastensis*), we used a paleofeces (RC L12 #1) collected at Rampart Cave (AZ, USA) and conserved at the Desert Lab at Arizona State University and collected by the late Paul S. Martin. For the giant ground sloth (*Megatherium americanum*), we had access to a rib bone sample (MAPB4R 3965) from Los Chaceras (Argentina) conserved in the Museo de la Asociación Paleontológica (Bariloche, Río Negro, Argentina). We also used three paleofeces from two different layers (C.2C_Layer 2, C.2E_Layer 4_1, C.2E_Layer 4_2) attributed to an undetermined Megatheriinae from Peñas de las Trampas 1.1 archeological site (Catamarca, Argentina) and deposited in the Institute of Archaeology and Museum of the National University of Tucumán (IAM-UNT; Tucumán, Argentina). Our analyses have shown that those paleofeces most likely came from the giant ground sloth (*Megatherium americanum*). Finally, for the two Caribbean sloths *Acratocnus ye* and *Parocnus serus*, we used a mandible with molars (UF 76365) and a bone (UF 75452) collected at two different localities from the Département de l'Ouest of the Republic of Haiti, respectively. Both samples are stored in the collections of the Florida Museum of Natural History (Gainesville, FL, USA).

METHOD DETAILS

Radiocarbon dating

Aliquots of freeze-dried ultrafiltered gelatin prepared from each sample were radiocarbon dated by the Keck Carbon Cycle AMS facility of the University of California Irvine (USA).

DNA extraction and library preparation from bone

Subsampling of bones was done in a dedicated ancient DNA laboratory facility at the McMaster Ancient DNA Centre for *Mylodon darwinii* MNHN 1905-4 (40 mg), *Mylodon darwinii* NHMUK PV M8758 (300 mg), *Acratocnus ye* UF 76365 (360 mg), *Parocnus serus* UF 75452 (360 mg), *Megalonyx jeffersonii* PMA P98.6.28 (300 mg), and *Megatherium americanum* MAPB4R 3965 for which three subsamples were taken from the rib cross section (187-285 mg). Each subsample was further reduced to small particle sizes of 1-5 mm using a hammer and chisel. The subsamples were then demineralized with 0.5 M EDTA (pH 8.0) for 24 h at room temperature with agitation, and the supernatant removed following centrifugation. The pellets were digested using a Tris-HCl-based (20 mM, pH 8.0) proteinase K (250 µg/ml) digestion solution with 0.5% sodium lauroyl sarcosinate (Fisher Scientific), 1% polyvinylpyrrolidone (PVP, Fisher scientific), 50 mM dithiothreitol (DTT), 2.5 mM N-phenacyl thiazolium bromide (PTB, Prime Organics), and 5 mM calcium chloride (CaCl2). Proteinase digestions were performed for 24 h at room temperature with agitation. Following centrifugation, the digestion supernatants were removed and pooled with the demineralization supernatants. This process was repeated three to four times, pooling supernatants with the original rounds. Organics were then extracted from the pooled supernatants using phenol:chloroform:isoamyl alcohol (PCI, 25:24:1), and the resulting post-centrifugation aqueous solution was again extracted with chloroform. The final aqueous solution was concentrated using 10 kDA Amicon centrifuge filters (Millipore) at 4000 x g or 14,000 x g depending on filter volume used (Amicon Ultra 0.5 ml or Amicon Ultra 4 ml), with up to four washes of 0.1x TE buffer (pH 8) to provide a final desalted concentrate of 50 µl. For *Megatherium americanum* MAPB4R 3965, demineralization and digestion were carried out similarly to other bone samples, with modifications based on in-house optimization. Pooled demineralization and digestion supernatants were extracted using the “Method B” extraction procedure outlined in Glocke and Meyer [54], except eluted off the column in 50 µl of EBT. Extraction blanks were carried alongside each sample during the entire extraction procedure to monitor for possible external contamination during handling.

Ancient DNA extracts and extraction blanks were finally purified with a MinElute column (Qiagen) to 50 µl EBT and converted to a double-stranded, Illumina sequencing library according to the protocol developed by Meyer and Kircher [55] with the following modifications: 1) the reaction volume for blunt-end repair was reduced to 40 µl with 25ul template; 2) all SPRI purification steps were substituted by spin column purification (MinElute PCR purification kit, Qiagen), and 3) adapter ligation was performed overnight at 16°C. For *Megatherium americanum* MAPB4R 3965, three libraries (L1043, L1044, and L1045) were generated from the three independent subsamples of the same specimen. These libraries were constructed from 20 µl of each purified extract as input in 40 µl reactions as above, with modifications in the End Repair step to accommodate the switch from NEBuffer 2 to NEBuffer 2.1, and the removal of Uracil-DNA glycosylase and Endonuclease VIII treatment.

DNA extraction and library preparation from paleofeces

Subsampling of paleofeces was performed in a dedicated ancient DNA laboratory facility at the McMaster Ancient DNA Centre for *Megatherium americanum* IAM-UNT C.2C_Layer2 (160 mg), *Megatherium americanum* IAM-UNT C.2E_Layer4_1 (140 mg), *Megatherium americanum* IAM-UNT C.2E_Layer4_2 (120 mg), and *Nothrotheriops shastensis* RC L12 #1 (130 mg). Using tweezers and scalpels subsamples were further reduced to small particle sizes of 1-5 mm. Each subsample was then incubated with a Guanidinium thiocyanate buffer (6 M GuSCN, 20 mM Tris (pH 8.0), 0.5% sodium lauroyl sarcosinate, 8 mM DTT, 4% PVP, and 10 mM PTB for 20 h at 37°C with agitation, and the supernatant removed following centrifugation. 500 µl of supernatant were then purified using MinElute columns eluting to a final volume of 25 µl with 0.1x TE plus 0.05 % Tween. Extraction blanks were carried alongside each sample during the entire extraction procedure to monitor for possible external contamination during handling.

584 Ancient DNA extracts and extraction blanks were converted into Illumina blunt-ended
585 libraries as described by Meyer and Kircher [55] with the following modifications: 1) the reaction
586 volume for blunt-end repair was reduced to 50 µl with 25 µl template; 2) buffer Tango (10x) was
587 substituted with NE Buffer 2 (10x); 3) BSA was added to the blunt-end repair reaction at a final
588 concentration of 0.1 mg/ml; 4) T4 polynucleotide kinase was reduced to a final concentration of
589 0.4 U/µl; 5) Uracil-DNA glycosylase and Endonuclease VIII were added to the blunt-end repair
590 reaction at a final concentration of 0.1 U/µl and 0.4 U/µl respectively; 6) the blunt-end repair
591 reaction was incubated at 37°C for 3 h without the addition of T4 DNA polymerase and again
592 after the addition of T4 DNA polymerase at a final concentration of 0.2U/µl at 25°C for 15 min
593 and 12°C for 15 min; 7) all SPRI purification steps were substituted by spin column purification
594 (MinElute PCR purification kit as suggested by Kircher et al. [56]); 8) adapter concentration in
595 the ligation reaction was reduced to 0.25 µM of each adapter as suggested by Kircher et al. [56];
596 9) adapter ligation was performed overnight at 16°C; 10) Bst polymerase was increased to a
597 final concentration of 0.4 U/µl; and 11) no purification step was performed after adapter fill-in
598 with Bst polymerase but instead, the enzyme was heat inactivated at 80°C for 20 min following
599 Kircher et al. [56].

600 **Library indexing, qPCR assay, target enrichment, and sequencing**

601 Constructed libraries were then double-indexed with P5 and P7 indexing primers [56] in a 50 µl
602 reaction containing 1x Herculase II Reaction Buffer, 250 µM each dNTP, 0.5x EvaGreen, 400
603 nM of each primer, 0.5 µl Herculase II Fusion DNA Polymerase, and 10 µl library. Cycling
604 conditions were 95°C for 2 min, 10 amplification cycles of (95°C for 15 sec, 60°C for 20 sec,
605 72°C for 30 sec), and a final extension of 72°C for 3 min. Amplifications were performed using a
606 MJ thermocycler (BioRad). Reactions were purified again with MinElute to 15 µL EBT. For
607 *Megatherium americanum* MAPB4R 3965, heat-deactivated libraries were indexed using 12.5 µl
608 of template with unique P5 and P7 indexes, with an increased primer concentration (750 nM)

609 and 1X KAPA SYBR®FAST qPCR Master Mix as this method produces less PCR artifacts than
610 Herculase II Fusion DNA Polymerase. To ensure that libraries contained endogenous DNA after
611 preparation, and that the blank extract libraries did not, each indexed library was subjected to a
612 quantitative PCR assay specifically targeting a 47 bp portion of the xenarthran mitochondrial
613 16S rRNA gene using primers Xen_16S_F2 and Xen_16S_R2 [21]. The following protocol
614 employing 1 µL of the library in a total reaction volume of 10 µl was used: 1x PCR Buffer II, 2.5
615 mM MgCl2, 250 µM dNTP mix, 1 mg/ml BSA, 250 nM each primer, 0.5x EvaGreen, 0.5 U
616 AmpliTaq Gold.

617 To maximize the capture of mitochondrial DNA from potentially divergent extinct sloth taxa,
618 the 5207 RNA baits previously designed using ancestral sequence reconstruction from a
619 representative sample of xenarthran mitogenomes were used [21]. These baits target the whole
620 mitogenome except the control region that is too repetitive to be reliably assembled with short
621 reads and too variable to be aligned among xenarthrans. The corresponding MYbaits targeted
622 enrichment kits were synthesized by Arbor Biosciences (https://arborbiosci.com/). A first round
623 of enrichment at 50°C was performed, followed by a second round at 55°C using 7.47 µl of
624 indexed library for 36-39 h, following the manufacturer's protocol. Phosphate-group end-blocked
625 oligonucleotides matching one strand of the regions flanking the 7 bp indexes of the library
626 adapters were included. A quantity of 25 ng of baits per reaction was used as it has been shown
627 to be sufficient for very sensitive capture of a small target region [57]. Following hybridization,
628 the reaction was cleaned according to the suggested protocol except that we used 200 µl rather
629 than 500 µl volumes of wash buffers for each wash step, to accommodate a 96-well plate-
630 format. Hot washes were performed at 50-55°C. The enriched library was eluted and then
631 purified with MinElute to 15 µl EBT, which we then re-amplified according to the protocol above
632 and again purified this time to 10 µl EBT. For *Megatherium americanum* MAPB4R 3965,

enrichment was carried out using the optimized protocol outlined in Karpinski et al. [58] using 5 µl of purified indexed library and 100 ng of bait set.

The enriched libraries were size-selected for fragment between 150 bp to 600 bp, pooled, and sequenced at McMaster Genomics Facility on the Illumina HiSeq 1500 system using the TruSeq Rapid (v1) chemistry with initial hybridization on the cBot. Each lane included a 1% spike-in of Illumina's PhiX v3 control library. Paired-end reads of either 2 x 90 bp (*Megatherium americanum* libraries) or 2 x 110 bp (all other libraries) were generated, along with dual 7 bp indexing on both runs.

Mitogenome assembly and annotation

Adapter and index tag sequences were trimmed from raw sequence reads using CutAdapt v1.16 [59]. Trimmed reads were then imported into Geneious Prime [60]. For each sample, reads were mapped against the *Homo sapiens* reference mitogenome sequence (NC_012920) using the “Low Sensitivity / Fastest” mapping strategy of Geneious Prime. Matching reads were excluded as human contamination and de novo assembly of the remaining reads was then performed using the metagenomic assembler MEGAHIT v1.1.1 [61]. Mitochondrial contigs were then identified by mapping MEGAHIT contigs of each sample against its closest reference xenarthran genome using the “High Sensitivity / Medium” mapping option of Geneious Prime. In the five cases for which multiple contigs were identified, draft partial mitogenomes were created by filling regions that lacked any coverage with question marks. Iterative mapping of deduplicated reads was then conducted using the “Low Sensitivity / Fastest” mapping strategy of Geneious Prime until there were no further improvements in extending coverage into the gap regions of the consensus sequence. The resulting partial mitogenomes were scanned by eye to check for the inclusion of any conflicting reads that might represent contaminants. The final partial mitogenomes were annotated by manually reporting annotations after pairwise alignment

with their closest xenarthran reference mitogenome using MAFFT v7.388 G-INSI [62] within Geneious Prime. The depth of coverage was estimated by remapping deduplicated reads to each partial mitogenome using the "Low Sensitivity / Fastest" mapping strategy of Geneious Prime.

DNA damage analyses

To check the authenticity of our newly obtained mitogenomes, we examined the patterns of DNA damage caused by post-mortem mutations using mapDamage v2.0.8 **[63]**. We screened our sequenced libraries for the presence of an excess of C-T and G-A transitions by mapping non-duplicated reads against their corresponding reconstructed consensus mitogenomes.

Mitogenomic dataset construction

We selected available mitogenomes for 25 living xenarthran species that are representative of the xenarthran diversity. We then added previously obtained mitogenomes from the extinct glyptodont (*Doedicurus* sp.) and extinct Darwin's ground sloth (*Mylodon darwinii*), as well as our 10 newly generated mitogenome sequences, and three afrotherian outgroup taxa. A careful comparison between our nearly complete *Nothrotheriops shastensis* mitogenome obtained from a paleofecal sample from Rampart Cave in Arizona and that of a partial mitogenome (9364 bp) from Gypsum Cave in Nevada produced by Slater et al. [20] revealed a number of discrepancies resulting in only 7183 identical sites between the two sequences. As most of these differences are likely the result of sequencing or assembly errors in the Slater et al. [20]'s *Nothrotheriops* sequence, as previously shown also for *Mylodon darwinii* [15], we have used our more complete and accurate sequences for these two taxa. All mitochondrial genes except the mitochondrial control region, which has not been sequenced for most of the extinct taxa, were extracted from the mitogenome annotations. The 24 tRNA and the two rRNA genes were then aligned at the nucleotide level using MAFFT G-INSI within Geneious Prime, and the translation-align option

was used to align the 13 protein-coding genes based on their amino acid sequences. Selection of unambiguously aligned sites was performed on each individual gene data set with Gblocks v0.91b [64] using default relaxed settings and the codon option for protein-coding genes. The final concatenation contained 15,157 unambiguously aligned nucleotide sites for 40 taxa.

Phylogenetic reconstructions

The best-fitting partition schemes and associated optimal models of sequence evolution were determined using both PartitionFinder v2.1.1 [65] and ModelFinder [66]. In both cases, the greedy algorithm was used starting from 42 a priori defined partitions corresponding to the three codon positions of the 13 protein-coding genes (3 x 13 = 39 partitions), the 12S (1) and 16S rRNAs (1), and all 24 concatenated tRNAs (1). Branch lengths have been unlinked and the Bayesian Information Criterion (BIC) was used for selecting the best-fitting partition scheme in all cases (Tables S1-S3). Maximum Likelihood reconstructions were conducted under the best-fitting partitioned models with both RAxML v8.1.22 [67] and IQ-TREE v1.6.6 [68] linking branches across the best-fitting partitions. Maximum Likelihood bootstrap values (BP_{RAxML} and $BP_{IQ\text{-}TREE}$) were computed by repeating the same ML heuristic search on 100 nonparametric bootstrap pseudo-replicates.

Bayesian phylogenetic inference under the best-fitting partition model was conducted using MrBayes v3.2.6 [69] with model parameters unlinked across partitions. Two independent runs of four incrementally heated Metropolis Coupling Markov Chain Monte Carlo (MCMCMC) starting from a random tree were performed. MCMCMC were run for 10,000,000 generations with trees and associated model parameters sampled every 1000 generations. The initial 2500 trees of each run were discarded as burn-in samples after convergence check as determined by monitoring the average standard deviation of split frequencies (ASDSF) between the two runs (ASDSF < 0.05) and effective sample size (ESS > 100) and potential scale reduction factor

(1.00 < PSRF < 1.02) values of the different parameters. The 50% majority-rule Bayesian consensus tree and associated clade posterior probabilities ($PP_{MrBayes}$) were then computed from the 15,000 combined trees sampled in the two independent runs.

Bayesian phylogenetic reconstruction was also conducted under the CAT-GTR+G4 mixture model using PhyloBayes MPI v1.7b [70]. Two independent Markov Chain Monte Carlo (MCMC) starting from a random tree were run for 18,000 cycles with trees and associated model parameters sampled every cycle. The initial 1800 trees (10%) sampled in each MCMC run were discarded as the burn-in after convergence checking by monitoring the ASDSF between the two independent runs (<0.05) and the effective sample sizes (ESS > 1000) of the different parameter values using PhyloBayes diagnostic tools *bpcomp* and *tracecomp*, respectively. The 50% majority-rule Bayesian consensus tree and the associated posterior probabilities ($PP_{PhyloBayes}$) was then computed using *bpcomp* from the remaining combined 32,400 (2 x 16,200) trees.

Molecular dating

Dating analyses were conducted using PhyloBayes v4.1c [71] under the site-heterogeneous CAT-GTR+G4 mixture model [72] and a relaxed clock model with a birth–death prior on divergence times [73] combined with soft fossil calibrations [74]. As calibration priors, we used five node intervals as determined from the fossil record following Gibb et al. [75]: 1) Paenungulata (maximum age 71.2 Mya, minimum age 55.6 Ma); 2) Xenarthra (maximum age 71.2 Mya, minimum age 58.5 Mya); 3) Pilosa (maximum age 65.5 Mya, minimum age 31.5 Mya); 4) Vermilingua (maximum age 61.1 Mya, minimum age 15.97 Ma); and 5) Tolypeutinae (maximum age 37.8 Mya, minimum age 23.0 Mya). The ancestral Folivora node was left unconstrained. The prior on the root of the tree (Placentalia) was set at 100 Mya according to

728 Meredith et al. [30]. The topology was fixed to the tree previously inferred in the RAxML, IQ-
729 TREE, and MrBayes analyses under the best fitting partition model.

730 Selection of the best-fitting clock model was performed using the cross-validation procedure
731 as implemented in PhyloBayes. The autocorrelated lognormal model (LN; [76], the uncorrelated
732 gamma (UGAM) relaxed clock model [77], and a strict molecular clock (CL) model were
733 compared. The cross-validation tests were performed by dividing the original alignment in a
734 learning set of 13,642 sites and a test set of 1515 sites. The overall procedure was randomly
735 replicated 10 times for which a MCMC chain was run on the learning set for a total 1100 cycles
736 sampling posterior rates and dates every cycle. The first 100 samples of each MCMC were
737 excluded as the burn-in period for calculating the cross-validation scores averaged across the
738 10 replicates in order to determine the number of time a given model fits the data better than the
739 reference model. Cross-validation tests indicated that both the autocorrelated lognormal (LN)
740 and the uncorrelated gamma (UGAM) models offered a much better fit to our mitogenomic
741 dataset than a strict molecular clock (CL) model (LN vs. CL: 32.5 ± 7.0; UGAM vs. CL: 29.3 ±
742 6.9). Between the two relaxed clock models, LN was the best fitting model (LN vs. UGAM: 3.2 ±
743 2.8).

744 The final dating calculations were conducted using PhyloBayes under the best-fitting CAT-
745 GTR+G mixture model and an autocorrelated lognormal relaxed clock with a birth–death prior
746 on divergence times combined with soft fossil calibrations. We run two independent MCMC
747 chains for a total 50,000 cycles sampling parameters every 10 cycles. The first 500 samples
748 (10%) of each MCMC were excluded as the burn-in after convergence diagnostics based on
749 ESS of parameters using *tracecomp*. Posterior estimates of divergence dates were then
750 computed from the remaining 4500 samples of each MCMC using the *readdiv* subprogram.
751 Posterior density plots of mean divergence times were then computed by using the R packages

ape v5.0 [78] to extract mean dates from sampled chronograms and ggridges v0.5.1 [79] to plot the overlapping distributions.

Ancestral reconstructions of dental characters

Maximum likelihood reconstruction of sloth phylogeny was performed on the morphological matrix of Varela et al. [12] using RAxML under the MK+GAMMA model with: 1) the same topological constraint that the original authors used in their Bayesian reconstructions, and 2) the molecular topology used as a backbone constraint. Maximum likelihood estimation of ancestral character states was then conducted for six dental characters using Mesquite v3.6 [80] using the Mk model on the two ML topologies previously obtained with RAxML. A similar investigation was realized using maximum parsimony for the tree search with the same matrix and constraints using PAUP* v4.0b10 [81] and for the estimation of ancestral character states using Mesquite. The six dental characters from Varela et al. [12] are: #6, diastema ([0] absent or rudimentary; [1] elongate); #13, size of Cf ([0] smallest tooth; [1] greatly enlarged; [2] neither the smallest nor enlarged); #14, size of cf ([0] smallest tooth; [1] greatly enlarged; [2] neither the smallest nor enlarged); #19, morphology of Cf/cf ([0] molariform; [2] caniniform; [3] incisiform); #21, position of Cf relative to the anterior edge of the maxilla ([0] right at the edge; [1] near the edge; [2] well-separated from the anterior edge); #23, fossa on palatal surface of maxilla posterior to Cf ([0] absent; [1] present).

High-resolution microtomography (microCT) of the skulls of a two-fingered sloth (*Choloepus didactylus* UM 789N; Université de Montpellier, France) and a three-fingered sloth (*Bradypus tridactylus* MZS 03557; Musée Zoologique de Strasbourg, France) was performed at the Montpellier Rio Imaging (MRI) platform using a Microtomograph RX EasyTom 150 with X-ray

source 40-150 kV. The 3D reconstructions of the skulls were performed with Avizo 9.4.0 (Visualization Sciences Group).

DATA AND SOFTWARE AVAILABILITY

Annotated mitogenomes have been deposited in GenBank (Accession Numbers MK903494-MK903503) and the corresponding raw Illumina reads in the European Nucleotide Archive (PRJEB32380). Additional data, including capture bait sequences, alignments, and trees can be retrieved from zenodo.org (DOI: 10.5281/zenodo.2658746).

REFERENCES

1. Woodburne, M.O. (2010). The Great American Biotic Interchange: Dispersals, Tectonics, Climate, Sea Level and Holding Pens. J. Mamm. Evol. *17*, 245–264.

2. Martin, P.S., and Klein, R.G. (1989). Quaternary Extinctions: A Prehistoric Revolution (University of Arizona Press).

3. White, J., and MacPhee, R. (2001). The sloths of the West Indies: A systematic and phylogenetic review. In Biogeography of the West Indies, C. Woods and F. Sergile, eds. (CRC Press), pp. 201–235.

4. Steadman, D.W., Martin, P.S., MacPhee, R.D.E., Jull, A.J.T., McDonald, H.G., Woods, C.A., Iturralde-Vinent, M., and Hodgins, G.W.L. (2005). Asynchronous extinction of late Quaternary sloths on continents and islands. Proc. Natl. Acad. Sci. *102*, 11763–11768.

5. MacPhee, R.D.E., Iturralde-Vinent, M.A., and Gaffney, E.S. (2003). Domo de Zaza, an Early Miocene vertebrate locality in South-Central Cuba, with notes on the

798 tectonic evolution of Puerto Rico and the Mona passage. Am. Mus. Novit. *3394*, 1–42.

799 6. MacPhee, R.D.E., and Iturralde-Vinent, M.A. (1995). Origin of the Greater
800 Antillean land mammal fauna, 1: New Tertiary fossils from Cuba and Puerto Rico. Am.
801 Mus. Novit. *3141*, 1–32.

802 7. Vélez-Juarbe, J., Martin, T., Macphee, R.D.E., and Ortega-Ariza, D. (2014). The
803 earliest Caribbean rodents: Oligocene caviomorphs from Puerto Rico. J. Vertebr.
804 Paleontol. *34*, 157–163.

805 8. Gaudin, T.J. (2004). Phylogenetic relationships among sloths (Mammalia,
806 Xenarthra, Tardigrada): the craniodental evidence. Zool. J. Linn. Soc. *140*, 255–305.

807 9. Pujos, F., Gaudin, T.J., De Iuliis, G., and Cartelle, C. (2012). Recent advances on
808 variability, morpho-functional adaptations, dental terminology, and evolution of sloths.
809 J. Mamm. Evol. *19*, 159–169.

810 10. Gaudin, T.J. (1995). The ear region of edentates and the phylogeny of the
811 Tardigrada (Mammalia, Xenarthra). J. Vertebr. Paleontol. *15*, 672–705.

812 11. Amson, E., Muizon, C., and Gaudin, T.J. (2017). A reappraisal of the phylogeny
813 of the Megatheria (Mammalia: Tardigrada), with an emphasis on the relationships of the
814 Thalassocninae, the marine sloths. Zool. J. Linn. Soc. *179*, 217–236.

815 12. Varela, L., Tambusso, P.S., McDonald, H.G., and Fariña, R.A. (2019). Phylogeny,
816 macroevolutionary trends and historical biogeography of sloths: insights from a
817 Bayesian morphological clock analysis. Syst. Biol. *68*, 204–218.

818 13. Pujos, F., De Iuliis, G., and Cartelle, C. (2017). A paleogeographic overview of
819 tropical fossil sloths: Towards an understanding of the origin of extant suspensory
820 sloths? J. Mamm. Evol. *24*, 19–38.

821 14. Höss, M., Dilling, A., Currant, A., and Pääbo, S. (1996). Molecular phylogeny of
822 the extinct ground sloth Mylodon darwinii. Proc. Natl. Acad. Sci. *93*, 181–185.

15. Delsuc, F., Kuch, M., Gibb, G.C., Hughes, J., Szpak, P., Southon, J., Enk, J., Duggan, A.T., and Poinar, H.N. (2018). Resolving the phylogenetic position of Darwin's extinct ground sloth (Mylodon darwinii) using mitogenomic and nuclear exon data. Proc. Biol. Sci. *285*.

16. Poinar, H.N., Hofreiter, M., Spaulding, W.G., Martin, P.S., Stankiewicz, B.A., Bland, H., Evershed, R.P., Possnert, G., and Pääbo, S. (1998). Molecular coproscopy: dung and diet of the extinct ground sloth Nothrotheriops shastensis. Science *281*, 402–406.

17. Hofreiter, M., Poinar, H.N., Spaulding, W.G., Bauer, K., Martin, P.S., Possnert, G., and Pääbo, S. (2000). A molecular analysis of ground sloth diet through the last glaciation. Mol. Ecol. *9*, 1975–1984.

18. Greenwood, A.D., Castresana, J., Feldmaier-Fuchs, G., and Pääbo, S. (2001). A molecular phylogeny of two extinct sloths. Mol. Phylogenet. Evol. *18*, 94–103.

19. Poinar, H., Kuch, M., McDonald, G., Martin, P., and Pääbo, S. (2003). Nuclear gene sequences from a late Pleistocene sloth coprolite. Curr. Biol. *13*, 1150–1152.

20. Slater, G.J., Cui, P., Forasiepi, A.M., Lenz, D., Tsangaras, K., Voirin, B., de Moraes-Barros, N., MacPhee, R.D.E., and Greenwood, A.D. (2016). Evolutionary relationships among extinct and extant sloths: the evidence of mitogenomes and retroviruses. Genome Biol. Evol. *8*, 607–621.

21. Delsuc, F., Gibb, G.C., Kuch, M., Billet, G., Hautier, L., Southon, J., Rouillard, J.-M., Fernicola, J.C., Vizcaíno, S.F., MacPhee, R.D., *et al.* (2016). The phylogenetic affinities of the extinct glyptodonts. Curr. Biol. *26*, R155–R156.

22. Martínez, J.G., Aschero, C.A., Powell, J.E., and Rodríguez, M.F. (2004). First evidence of extinct megafauna in the Southern Argentinian puna. Curr. Res. Pleistocene *21*, 104–107.

23. Martínez, J.G. (2014). Contributions to the knowledge of natural history and

archaeology of hunter-gatherers of Antofagasta de la Sierra (southern Argentinian puna): the case of Peñas de las Trampas 1.1. In Hunter-gatherers from a high-altitude desert. People of the Salt Puna (northwest Argentina). BAR International Series. Oxford: Archaeopress, E. L. Pintar, ed., pp. 71–93.

24. Ruiz-García, M., Chacón, D., Plese, T., Schuler, I., and Shostell, J.M. (2018). Mitogenomics phylogenetic relationships of the current sloth's genera and species (Bradypodidae and Megalonychidae). Mitochondrial DNA Part A *29*, 281–299.

25. Rohland, N., Harney, E., Swapan, M., Nordenfelt, S., and Reich, D. (2015). Partial uracil–DNA–glycosylase treatment for screening of ancient DNA. Philos. Trans. R. Soc. B Biol. Sci. *370*, 20130624.

26. Li, G., Davis, B.W., Eizirik, E., and Murphy, W.J. (2016). Phylogenomic evidence for ancient hybridization in the genomes of living cats (Felidae). Genome Res. *26*, 1–11.

27. Kumar, V., Lammers, F., Bidon, T., Pfenninger, M., Kolter, L., Nilsson, M.A., and Janke, A. (2017). The evolutionary history of bears is characterized by gene flow across species. Sci. Rep. *7*, 46487.

28. Presslee, S., Slater, G., Pujos, F., Forasiepi, A.M., Fischer, R., Molloy, K., Mackie, M., Olsen, J.V., Kramarz, A., Taglioretti, M., *et al.* (2019). Collagen proteomics provides novel insights into relationships of tree sloths and their extinct relatives. Nat. Ecol. Evol. *In press*.

29. Pujos, F., De Iuliis, G., Argot, C., and Werdelin, L. (2007). A peculiar climbing Megalonychidae from the Pleistocene of Peru and its implication for sloth history. Zool. J. Linn. Soc. *149*, 179–235.

30. Meredith, R.W., Janečka, J.E., Gatesy, J., Ryder, O.A., Fisher, C.A., Teeling, E.C., Goodbla, A., Eizirik, E., Simão, T.L.L., Stadler, T., *et al.* (2011). Impacts of the Cretaceous terrestrial revolution and KPg extinction on mammal diversification. Science *334*, 521–524.

31. Springer, M.S., Meredith, R.W., Teeling, E.C., and Murphy, W.J. (2013). Technical Comment on "The Placental Mammal Ancestor and the Post–K-Pg Radiation of Placentals." Science *341*, 613–613.

32. Hautier, L., Gomes Rodrigues, H., Billet, G., and Asher, R.J. (2016). The hidden teeth of sloths: evolutionary vestiges and the development of a simplified dentition. Sci. Rep. *6*, 27763.

33. McKenna, M.C., Wyss, A.R., and Flynn, J.J. (2006). Paleogene pseudoglyptodont xenarthrans from Central Chile and Argentine Patagonia. Am. Mus. Novit., 1–18.

34. McKenna, M.C., and Bell, S.K. (1997). Classification of mammals: above the species level (Columbia University Press).

35. Guth, C. (1961). La région temporale des Edentés.

36. Patterson, B., and Pascual, R. (1968). The fossil mammal fauna of South America. Q. Rev. Biol. *43*, 409–451.

37. Webb, S.D. (1985). The interrelationships of tree sloths and ground sloths. In The evolution and ecology of armadillos, sloths, and vermilinguas, pp. 105–112.

38. Colwyn, D.A., and Hren, M.T. (2019). An abrupt decrease in Southern Hemisphere terrestrial temperature during the Eocene–Oligocene transition. Earth Planet. Sci. Lett. *512*, 227–235.

39. Dunn, R.E., Strömberg, C.A.E., Madden, R.H., Kohn, M.J., and Carlini, A.A. (2015). Linked canopy, climate, and faunal change in the Cenozoic of Patagonia. Science *347*, 258–261.

40. McDonald, H.G., and De Iuliis, G. (2008). Fossil history of sloths. In The biology of the Xenarthra, S. F. Vizcaíno and W. J. Loughry, eds. (University Press of Florida), pp. 39–55.

41. Iturralde-Vinent, M., and MacPhee, R.D. (1999). Paleogeography of the

900 Caribbean region: implications for Cenozoic biogeography. Bull. Am. Mus. Nat. Hist.
901 *238*, 1–95.

902 42. MacPhee, R.D.E., and Iturralde-Vinent, M.A. (1994). First Tertiary land mammal
903 from Greater Antilles: an Early Miocene sloth (Xenarthra, Megalonychidae) from Cuba.
904 Am. Mus. Novit., 13.

905 43. Brace, S., Thomas, J.A., Dalén, L., Burger, J., MacPhee, R.D.E., Barnes, I., and
906 Turvey, S.T. (2016). Evolutionary history of the Nesophontidae, the last unplaced recent
907 mammal family. Mol. Biol. Evol. *33*, 3095–3103.

908 44. Springer, M.S., Murphy, W.J., and Roca, A.L. (2018). Appropriate fossil
909 calibrations and tree constraints uphold the Mesozoic divergence of solenodons from
910 other extant mammals. Mol. Phylogenet. Evol. *121*, 158–165.

911 45. Fabre, P.-H., Vilstrup, J.T., Raghavan, M., Der Sarkissian, C., Willerslev, E.,
912 Douzery, E.J.P., and Orlando, L. (2014). Rodents of the Caribbean: origin and
913 diversification of hutias unravelled by next-generation museomics. Biol. Lett. *10*,
914 20140266.

915 46. Brace, S., Turvey, S.T., Weksler, M., Hoogland, M.L.P., and Barnes, I. (2015).
916 Unexpected evolutionary diversity in a recently extinct Caribbean mammal radiation.
917 Proc. R. Soc. B Biol. Sci. *282*, 20142371.

918 47. Woods, R., Turvey, S.T., Brace, S., MacPhee, R.D.E., and Barnes, I. (2018).
919 Ancient DNA of the extinct Jamaican monkey Xenothrix reveals extreme insular change
920 within a morphologically conservative radiation. Proc. Natl. Acad. Sci., 201808603.

921 48. Alonso, R., Crawford, A.J., and Bermingham, E. (2012). Molecular phylogeny of
922 an endemic radiation of Cuban toads (Bufonidae: Peltophryne) based on mitochondrial
923 and nuclear genes: Origin and diversification of Cuban toads. J. Biogeogr. *39*, 434–451.

924 49. Crews, S.C., and Gillespie, R.G. (2010). Molecular systematics of Selenops
925 spiders (Araneae: Selenopidae) from North and Central America: implications for

926 Caribbean biogeography. Biol. J. Linn. Soc. *101*, 288–322.

927 50. Chamberland, L., McHugh, A., Kechejian, S., Binford, G.J., Bond, J.E.,
928 Coddington, J., Dolman, G., Hamilton, C.A., Harvey, M.S., Kuntner, M., *et al.* (2018).
929 From Gondwana to GAARlandia: Evolutionary history and biogeography of ogre-faced
930 spiders (Deinopis). J. Biogeogr. *45*, 2442–2457.

931 51. Tong, Y., Binford, G., Rheims, C.A., Kuntner, M., Liu, J., and Agnarsson, I.
932 (2019). Huntsmen of the Caribbean: Multiple tests of the GAARlandia hypothesis. Mol.
933 Phylogenet. Evol. *130*, 259–268.

934 52. Pant, S.R., Goswami, A., and Finarelli, J.A. (2014). Complex body size trends in
935 the evolution of sloths (Xenarthra: Pilosa). BMC Evol. Biol. *14*. Available at:
936 http://bmcevolbiol.biomedcentral.com/articles/10.1186/s12862-014-0184-1 [Accessed
937 October 10, 2018].

938 53. Toledo, N., Bargo, M.S., Vizcaíno, S.F., De Iuliis, G., and Pujos, F. (2017).
939 Evolution of body size in anteaters and sloths (Xenarthra, Pilosa): phylogeny,
940 metabolism, diet and substrate preferences. Earth Environ. Sci. Trans. R. Soc. Edinb.
941 *106*, 289–301.

942 54. Glocke, I., and Meyer, M. (2017). Extending the spectrum of DNA sequences
943 retrieved from ancient bones and teeth. Genome Res. *27*, 1230–1237.

944 55. Meyer, M., and Kircher, M. (2010). Illumina sequencing library preparation for
945 highly multiplexed target capture and sequencing. Cold Spring Harb. Protoc. *2010*,
946 pdb.prot5448.

947 56. Kircher, M., Sawyer, S., and Meyer, M. (2012). Double indexing overcomes
948 inaccuracies in multiplex sequencing on the Illumina platform. Nucleic Acids Res. *40*, e3.

949 57. Enk, J., Rouillard, J.-M., and Poinar, H. (2013). Quantitative PCR as a predictor of
950 aligned ancient DNA read counts following targeted enrichment. BioTechniques *55*,
951 300–309.

952 58. Karpinski, E., Mead, J.I., and Poinar, H.N. (2017). Molecular identification of
953 paleofeces from Bechan Cave, southeastern Utah, USA. Quat. Int. *443*, 140–146.

954 59. Martin, M. (2011). Cutadapt removes adapter sequences from high-throughput
955 sequencing reads. EMBnet.journal *17*, 10–12.

956 60. Kearse, M., Moir, R., Wilson, A., Stones-Havas, S., Cheung, M., Sturrock, S.,
957 Buxton, S., Cooper, A., Markowitz, S., Duran, C., *et al.* (2012). Geneious Basic: An
958 integrated and extendable desktop software platform for the organization and analysis
959 of sequence data. Bioinformatics *28*, 1647–1649.

960 61. Li, D., Luo, R., Liu, C.-M., Leung, C.-M., Ting, H.-F., Sadakane, K., Yamashita, H.,
961 and Lam, T.-W. (2016). MEGAHIT v1.0: A fast and scalable metagenome assembler
962 driven by advanced methodologies and community practices. Methods San Diego Calif
963 *102*, 3–11.

964 62. Katoh, K., Kuma, K., Toh, H., and Miyata, T. (2005). MAFFT version 5:
965 improvement in accuracy of multiple sequence alignment. Nucleic Acids Res. *33*, 511–
966 518.

967 63. Jónsson, H., Ginolhac, A., Schubert, M., Johnson, P.L.F., and Orlando, L. (2013).
968 mapDamage2.0: fast approximate Bayesian estimates of ancient DNA damage
969 parameters. Bioinformatics *29*, 1682–1684.

970 64. Castresana, J. (2000). Selection of conserved blocks from multiple alignments for
971 their use in phylogenetic analysis. Mol. Biol. Evol. *17*, 540–552.

972 65. Lanfear, R., Frandsen, P.B., Wright, A.M., Senfeld, T., and Calcott, B. (2017).
973 PartitionFinder 2: new methods for selecting partitioned models of evolution for
974 molecular and morphological phylogenetic analyses. Mol. Biol. Evol. *34*, 772–773.

975 66. Kalyaanamoorthy, S., Minh, B.Q., Wong, T.K., von Haeseler, A., and Jermiin, L.S.
976 (2017). ModelFinder: fast model selection for accurate phylogenetic estimates. Nat.
977 Methods *14*, 587.

978 67. Stamatakis, A. (2014). RAxML version 8: a tool for phylogenetic analysis and
979 post-analysis of large phylogenies. Bioinformatics *30*, 1312–1313.

980 68. Nguyen, L.-T., Schmidt, H.A., von Haeseler, A., and Minh, B.Q. (2015). IQ-TREE:
981 a fast and effective stochastic algorithm for estimating maximum-likelihood phylogenies.
982 Mol. Biol. Evol. *32*, 268–274.

983 69. Ronquist, F., Teslenko, M., van der Mark, P., Ayres, D.L., Darling, A., Höhna, S.,
984 Larget, B., Liu, L., Suchard, M.A., and Huelsenbeck, J.P. (2012). MrBayes 3.2: Efficient
985 Bayesian phylogenetic inference and model choice across a large model space. Syst.
986 Biol. *61*, 539–542.

987 70. Lartillot, N., Rodrigue, N., Stubbs, D., and Richer, J. (2013). PhyloBayes MPI:
988 phylogenetic reconstruction with infinite mixtures of profiles in a parallel environment.
989 Syst. Biol. *62*, 611–615.

990 71. Lartillot, N., Lepage, T., and Blanquart, S. (2009). PhyloBayes 3: a Bayesian
991 software package for phylogenetic reconstruction and molecular dating. Bioinformatics
992 *25*, 2286–2288.

993 72. Lartillot, N., and Philippe, H. (2004). A Bayesian mixture model for across-site
994 heterogeneities in the amino-acid replacement process. Mol. Biol. Evol. *21*, 1095–1109.

995 73. Gernhard, T. (2008). The conditioned reconstructed process. J. Theor. Biol. *253*,
996 769–778.

997 74. Rannala, B., and Yang, Z. (2007). Inferring speciation times under an episodic
998 molecular clock. Syst. Biol. *56*, 453–466.

999 75. Gibb, G.C., Condamine, F.L., Kuch, M., Enk, J., Moraes-Barros, N., Superina, M.,
1000 Poinar, H.N., and Delsuc, F. (2016). Shotgun mitogenomics provides a reference
1001 phylogenetic framework and timescale for living xenarthrans. Mol. Biol. Evol. *33*, 621–
1002 642.

1003 76. Thorne, J.L., Kishino, H., and Painter, I.S. (1998). Estimating the rate of

evolution of the rate of molecular evolution. Mol. Biol. Evol. *15*, 1647–1657.

77. Drummond, A.J., Ho, S.Y.W., Phillips, M.J., and Rambaut, A. (2006). Relaxed phylogenetics and dating with confidence. PLoS Biol. *4*, e88.

78. Paradis, E., and Schliep, K. (2019). ape 5.0: an environment for modern phylogenetics and evolutionary analyses in R. Bioinformatics *35*, 526–528.

79. Wilke, C.O. (2017). Ggridges: Ridgeline plots in'ggplot2'. R Package Version 04.

80. Maddison, W., and Maddison, D. (2001). Mesquite: a modular system for evolutionary analysis.

81. Swofford, D.L. (2001). PAUP*: Phylogenetic analysis using parsimony (and other methods) 4.0. B5.

Species	Common name	Family	Sample type	Radiocarbon 14C age BP	Museum	Specimen voucher	Library	Origin	Mean read length (bp)	Mean coverage	MEGAHIT mito Contigs
Mylodon darwinii	Darwin's ground sloth	Mylodontidae	HP1502 Skin with osteoderms	13,360 ± 40	Muséum National d'Histoire Naturelle (Paris, France)	MNHN 1905-4	Lib_16	Mylodon Cave (Última Esperanza, Chile)	44.5	567X	5
Mylodon darwinii	Darwin's ground sloth	Mylodontidae	HP1554 Bone	12,880 ± 35	Natural History Museum (London, UK)	NHMUK PV M8758	Lib_67	Mylodon Cave (Última Esperanza, Chile)	54.3	465X	1
Megalonyx jeffersonii	Jefferson's ground sloth	Megalonychidae	HP1652 Bone	45,800 ± 2000	Academy of Natural Sciences of Drexel University (Philadelphia, PA, USA)	PMA P98.6.28	Lib_69	Big Bone Cave (TN, USA)	56.2	271X	1
Nothrotheriops shastensis	Shasta ground sloth	Nothrotheriidae	HP1904 Paleofeces	28,460 ± 320	The Desert Lab, Arizona State University (Tempe, AZ, USA)	RC L12 #1	Lib_X32	Rampart cave (AZ, USA)	88.4	402X	1
Megatherium americanum	Giant ground sloth	Megatheriidae	HP3613 Rib bone	19,050 ± 80	Museo de la Asociación Paleontológica (Bariloche, Argentina)	MAPB4R 3965	Lib_1043, Lib_1044, Lib_1045	Los Chaceras (Bariloche, Argentina)	57.5	2277X	4
Megatherium americanum	Giant ground sloth	Megatheriidae	HP2087 Paleofeces	12,920 ± 190 - 12,510 ± 240*	Institute of Archaeology and Museum of the National University of Tucumán (Tucumán, Argentina)	C.2C_Layer 2	Lib_X18	Peñas de las Trampas 1.1 (Catamarca, Argentina)	93.9	192X	1
Megatherium americanum	Giant ground sloth	Megatheriidae	HP2093 Paleofeces	19,610 ± 290*	Institute of Archaeology and Museum of the National University of Tucumán (Tucumán, Argentina)	C.2E_Layer 4_1	Lib_X23	Peñas de las Trampas 1.1 (Catamarca, Argentina)	63.2	108X	7
Megatherium americanum	Giant ground sloth	Megatheriidae	HP2095 Paleofeces	19,610 ± 290*	Institute of Archaeology and Museum of the National University of Tucumán (Tucumán, Argentina)	C.2E_Layer 4_2	Lib_X25	Peñas de las Trampas 1.1 (Catamarca, Argentina)	81.8	335X	1
Acratocnus ye	Hispaniolan ground sloth	Acratocnidae	HP1655 Mandible with molar	10,395 ± 40	Florida Museum of Natural History (Gainesville, FL, USA)	UF 76365	Lib_58	Trouing de la Scierie (Département de l'Ouest, Republic of Haiti)	49.6	135X	10

Parocnus serus	Greater Haitian ground sloth	Parocnidae	HP1602 Bone	NA	Florida Museum of Natural History (Gainesville, FL, USA)	UF 75452	Lib_54	Trouing Marassa (Département de l'Ouest, Republic of Haiti)	55.2	66X	17

* dated by Martínez [23]. NA : not available.

Figure 1

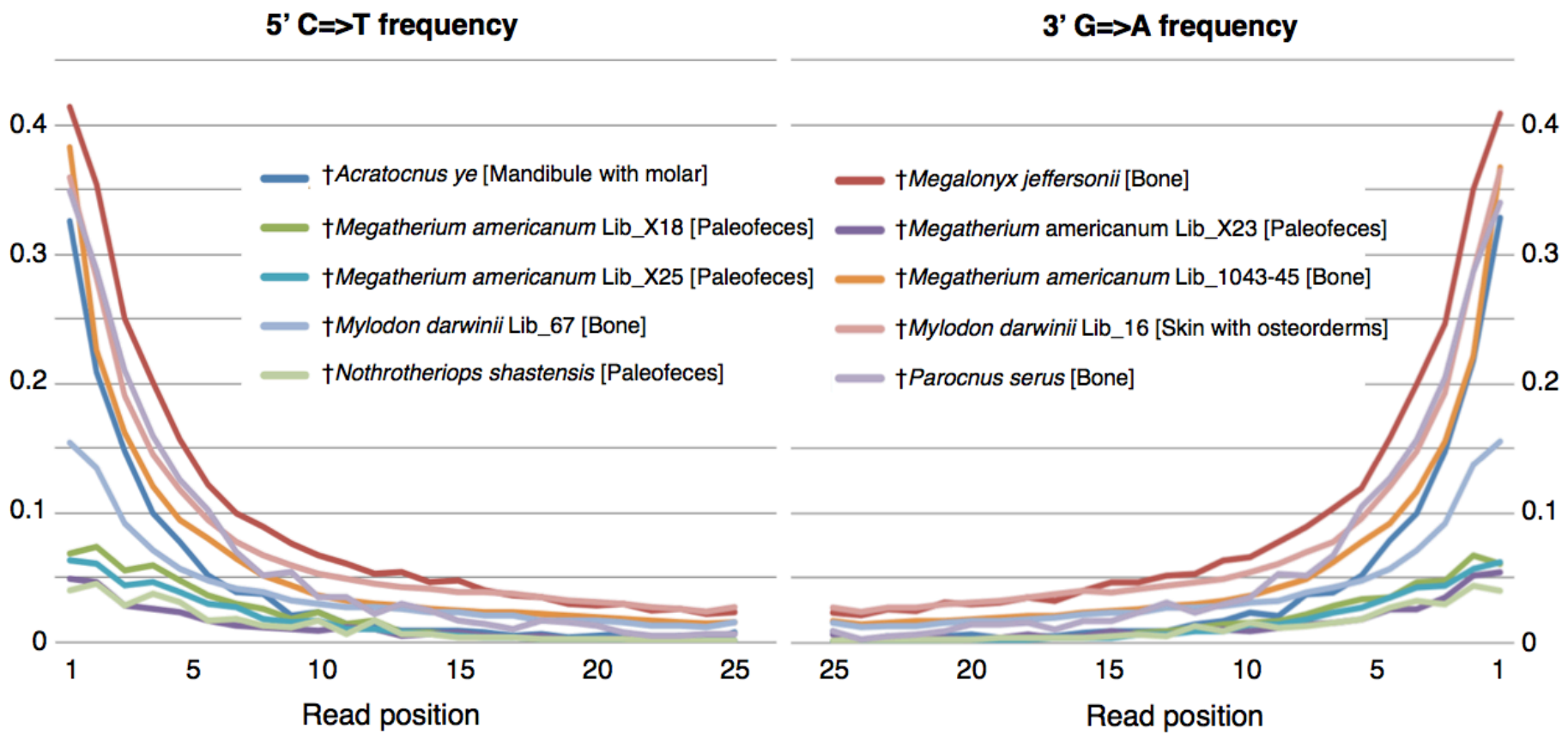
5' C=>T frequency
3' G=>A frequency
†Acratocnus ye [Mandibule with molar]
†Megatherium americanum Lib_X18 [Paleofeces]
†Megatherium americanum Lib_X25 [Paleofeces]
†Mylodon darwinii Lib_67 [Bone]
†Nothrotheriops shastensis [Paleofeces]
†Megalonyx jeffersonii [Bone]
†Megatherium americanum Lib_X23 [Paleofeces]
†Megatherium americanum Lib_1043-45 [Bone]
†Mylodon darwinii Lib_16 [Skin with osteorderms]
†Parocnus serus [Bone]
0.4
0.3
0.2
0.1
0
1
5
10
15
20
25
Read position

Figure 2

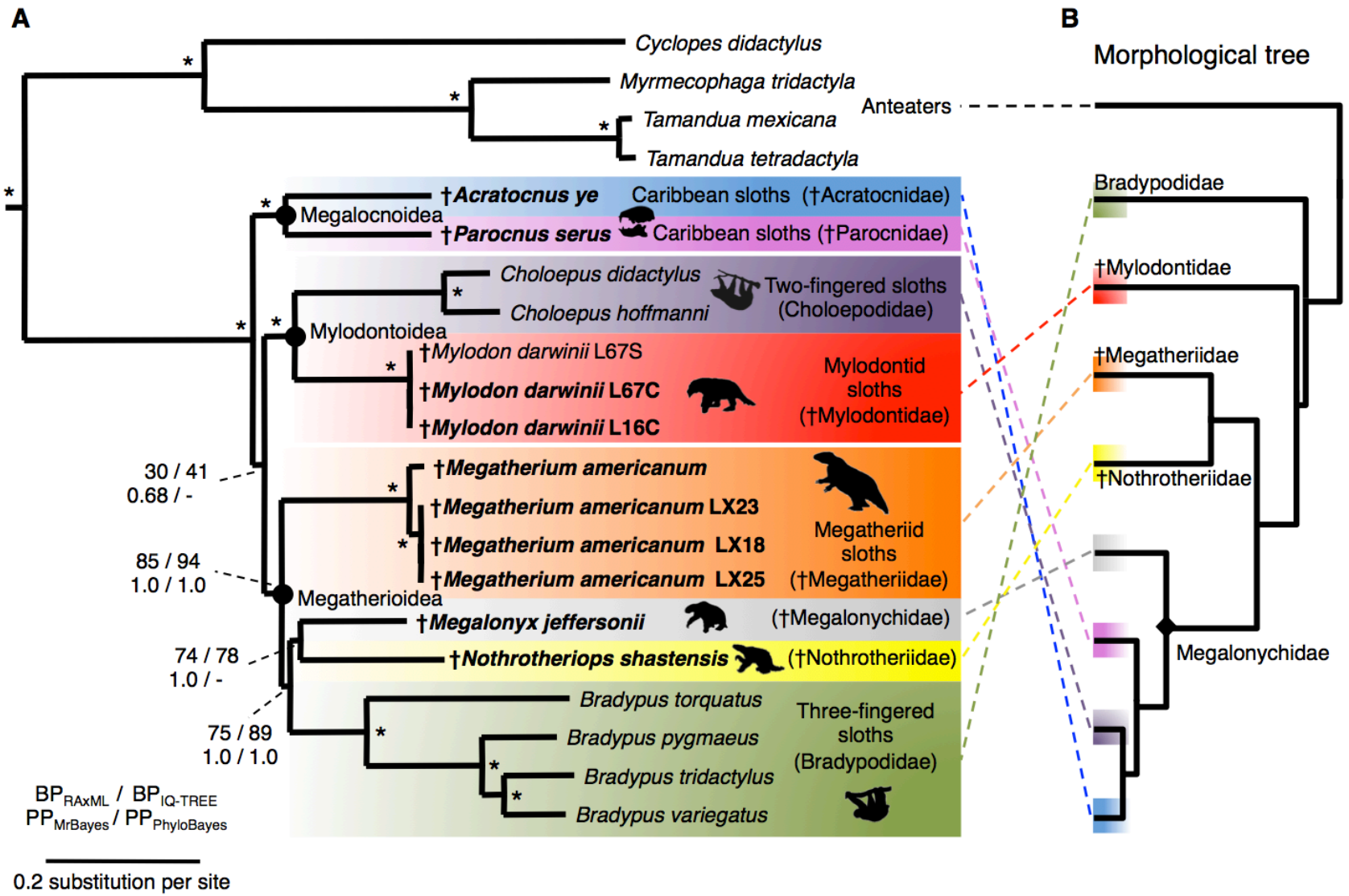
A
B
Morphological tree
Cyclopes didactylus
Myrmecophaga tridactyla
Tamandua mexicana
Tamandua tetradactyla
Anteaters
†Acratocnus ye
Caribbean sloths (†Acratocnidae)
Megalocnoidea
†Parocnus serus
Caribbean sloths (†Parocnidae)
Choloepus didactylus
Choloepus hoffmanni
Two-fingered sloths (Choloepodidae)
Mylodontoidea
†Mylodon darwinii L67S
†Mylodon darwinii L67C
†Mylodon darwinii L16C
Mylodontid sloths (†Mylodontidae)
30 / 41
0.68 / -
†Megatherium americanum
†Megatherium americanum LX23
†Megatherium americanum LX18
†Megatherium americanum LX25
Megatheriid sloths (†Megatheriidae)
85 / 94
1.0 / 1.0
Megatherioidea
†Megalonyx jeffersonii
(†Megalonychidae)
74 / 78
1.0 / -
†Nothrotheriops shastensis
(†Nothrotheriidae)
75 / 89
1.0 / 1.0
Bradypus torquatus
Bradypus pygmaeus
Bradypus tridactylus
Bradypus variegatus
Three-fingered sloths (Bradypodidae)
BP RAxML / BP IQ-TREE
PP MrBayes / PP PhyloBayes
0.2 substitution per site
Bradypodidae
†Mylodontidae
†Megatheriidae
†Nothrotheriidae
Megalonychidae

Figure 3

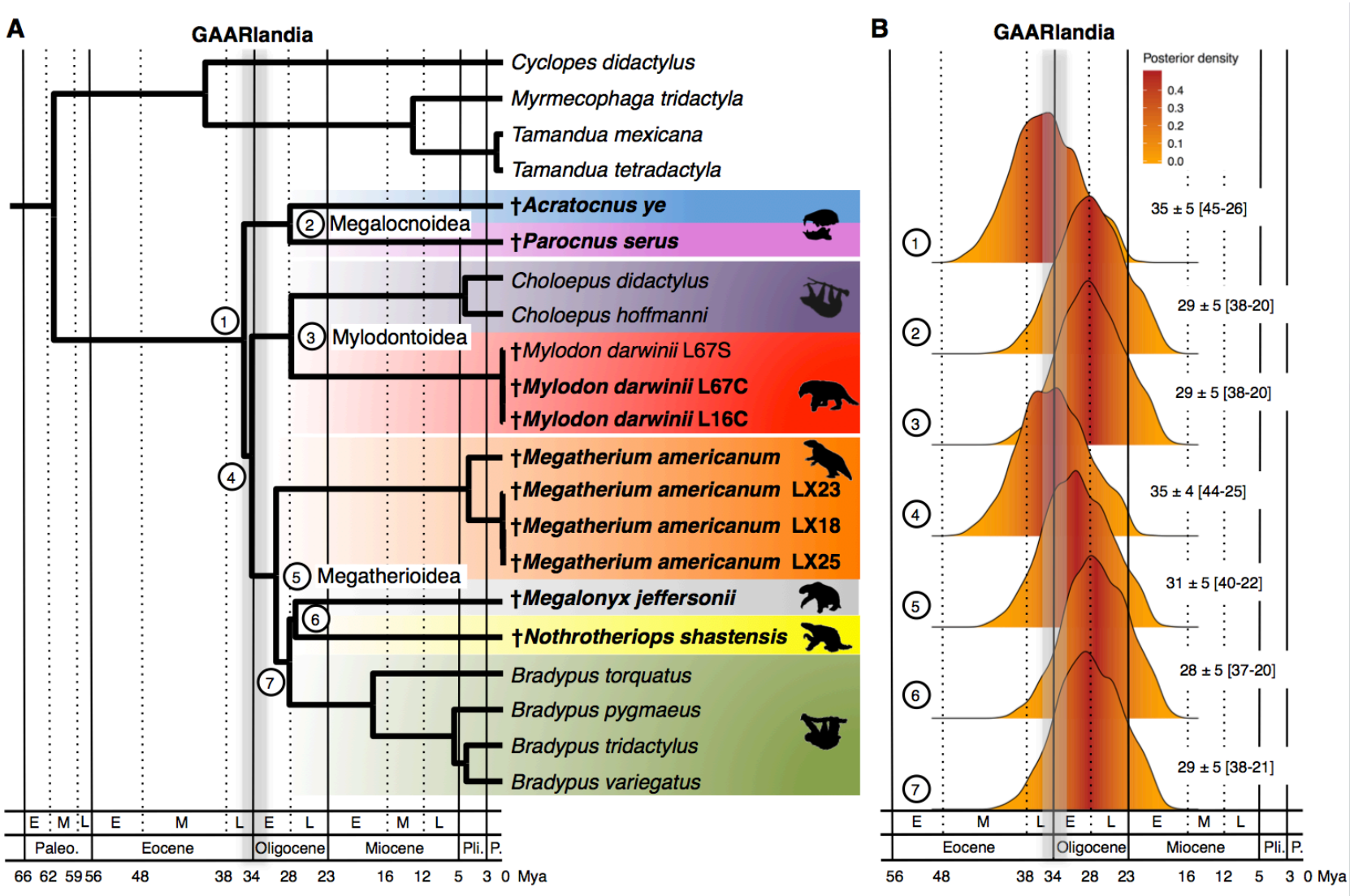
A
GAARlandia
Cyclopes didactylus
Myrmecophaga tridactyla
Tamandua mexicana
Tamandua tetradactyla
†Acratocnus ye
†Parocnus serus
Megalocnoidea
Choloepus didactylus
Choloepus hoffmanni
Mylodontoidea
†Mylodon darwinii L67S
†Mylodon darwinii L67C
†Mylodon darwinii L16C
†Megatherium americanum
†Megatherium americanum LX23
†Megatherium americanum LX18
†Megatherium americanum LX25
Megatherioidea
†Megalonyx jeffersonii
†Nothrotheriops shastensis
Bradypus torquatus
Bradypus pygmaeus
Bradypus tridactylus
Bradypus variegatus
E M L E M L E L E M L
Paleo. Eocene Oligocene Miocene Pli. P.
66 62 59 56 48 38 34 28 23 16 12 5 3 0 Mya
B
GAARlandia
Posterior density
0.4
0.3
0.2
0.1
0.0
35 ± 5 [45-26]
29 ± 5 [38-20]
29 ± 5 [38-20]
35 ± 4 [44-25]
31 ± 5 [40-22]
28 ± 5 [37-20]
29 ± 5 [38-21]
E M L E L E M L
Eocene Oligocene Miocene Pli. P.
56 48 38 34 28 23 16 12 5 3 0 Mya

Figure 4

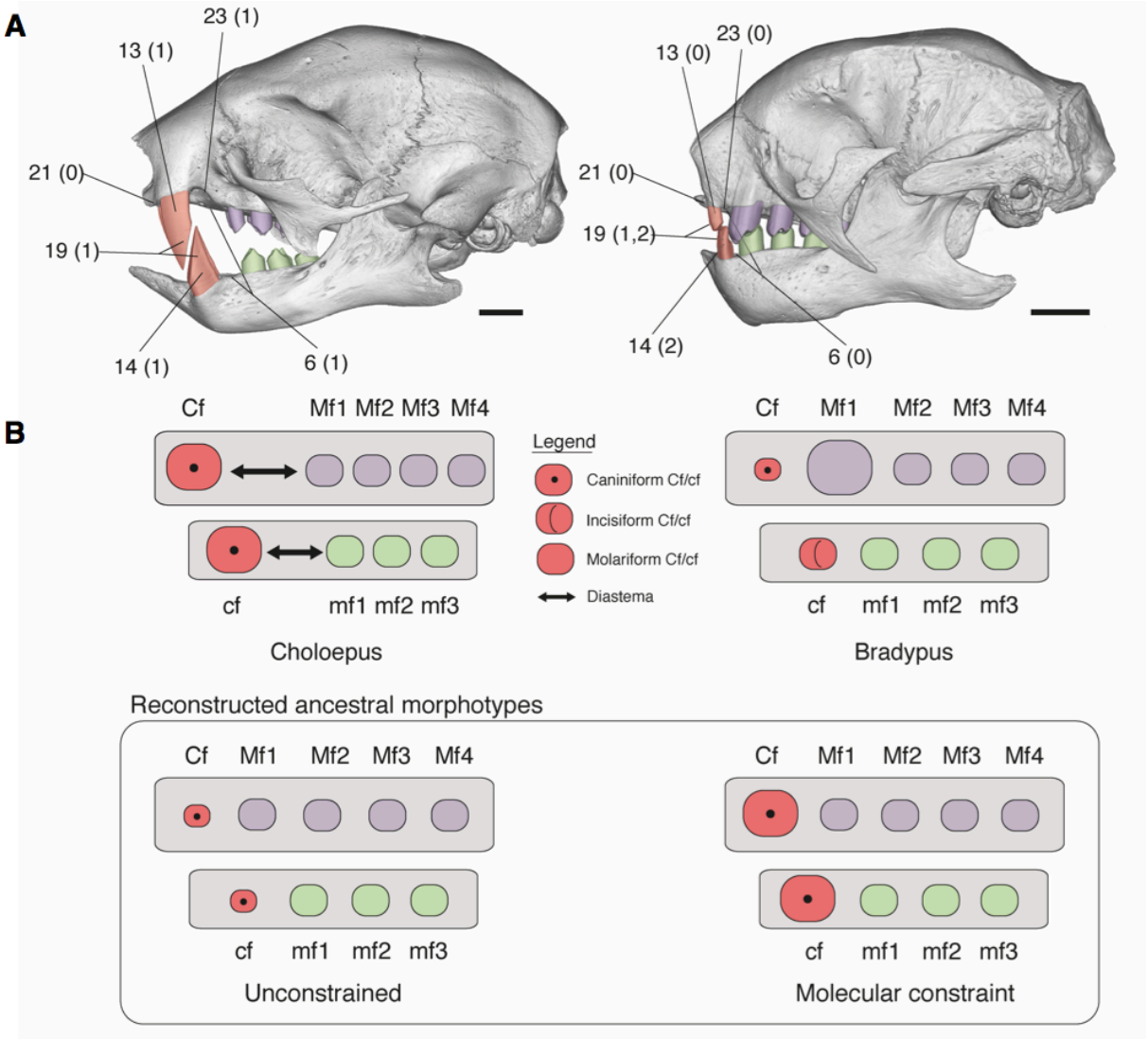
A
23 (1)
13 (1)
21 (0)
19 (1)
14 (1)
6 (1)
23 (0)
13 (0)
21 (0)
19 (1,2)
14 (2)
6 (0)
B
Cf
Mf1 Mf2 Mf3 Mf4
cf
mf1 mf2 mf3
Choloepus
Legend
Caniniform Cf/cf
Incisiform Cf/cf
Molariform Cf/cf
Diastema
Cf
Mf1
Mf2
Mf3
Mf4
cf
mf1
mf2
mf3
Bradypus
Reconstructed ancestral morphotypes
Unconstrained
Molecular constraint

Figure 5

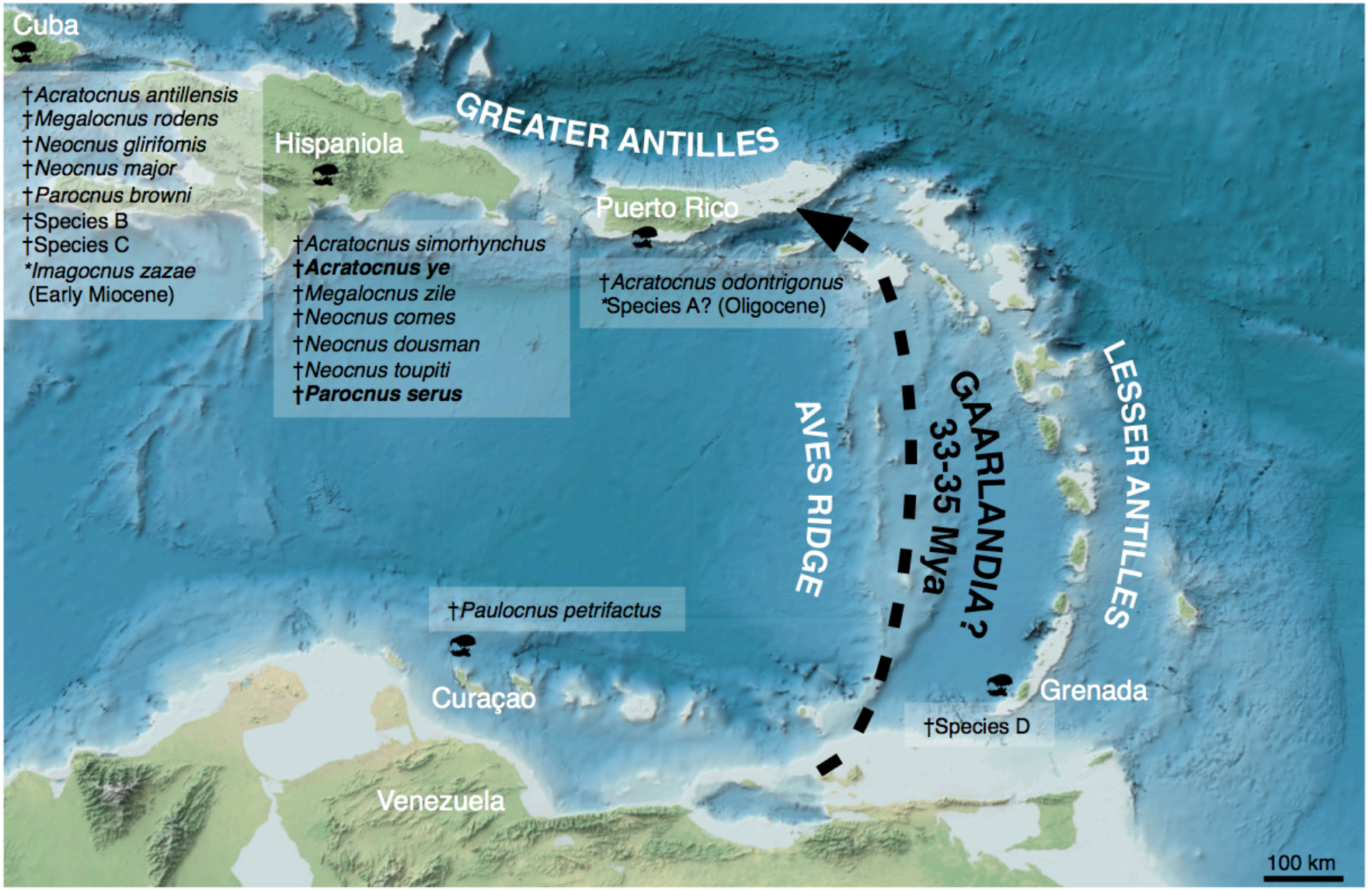
Cuba
†Acratocnus antillensis
†Megalocnus rodens
†Neocnus glirifomis
†Neocnus major
†Parocnus browni
†Species B
†Species C
*Imagocnus zazae
(Early Miocene)
Hispaniola
GREATER ANTILLES
Puerto Rico
†Acratocnus simorhynchus
†Acratocnus ye
†Megalocnus zile
†Neocnus comes
†Neocnus dousman
†Neocnus toupiti
†Parocnus serus
†Acratocnus odontrigonus
*Species A? (Oligocene)
AVES RIDGE
GAARLANDIA?
33-35 Mya
LESSER ANTILLES
†Paulocnus petrifactus
Curaçao
Grenada
†Species D
Venezuela
100 km

Current Biology, Volume *29*

Supplemental Information

Ancient Mitogenomes Reveal the Evolutionary History and Biogeography of Sloths

Frédéric Delsuc, Melanie Kuch, Gillian C. Gibb, Emil Karpinski, Dirk Hackenberger, Paul Szpak, Jorge G. Martínez, Jim I. Mead, H. Gregory McDonald, Ross D.E. MacPhee, Guillaume Billet, Lionel Hautier, and Hendrik N. Poinar

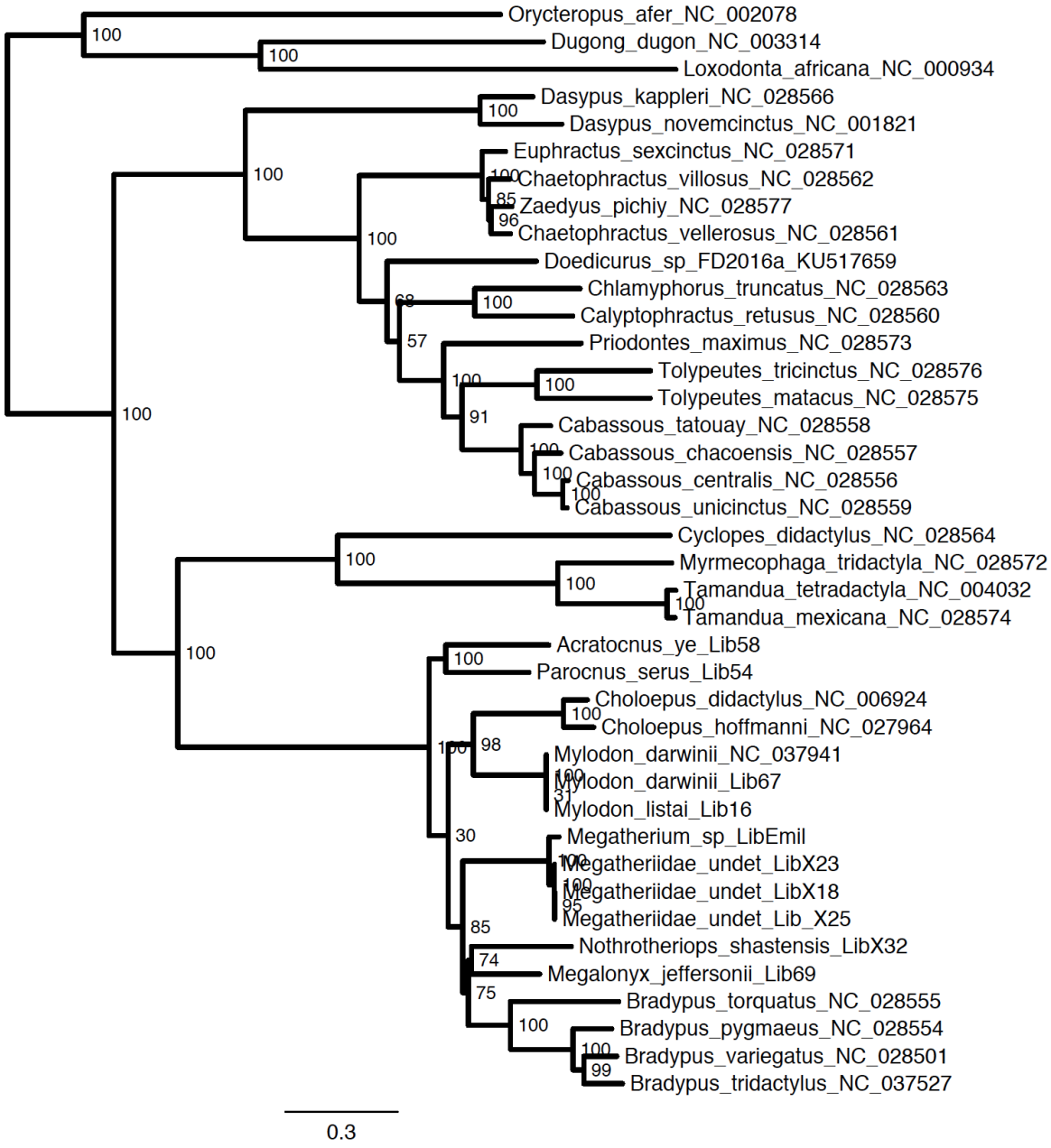
Orycteropus_afer_NC_002078
Dugong_dugon_NC_003314
Loxodonta_africana_NC_000934
Dasypus_kappleri_NC_028566
Dasypus_novemcinctus_NC_001821
Euphractus_sexcinctus_NC_028571
Chaetophractus_villosus_NC_028562
Zaedyus_pichiy_NC_028577
Chaetophractus_vellerosus_NC_028561
Doedicurus_sp_FD2016a_KU517659
Chlamyphorus_truncatus_NC_028563
Calyptophractus_retusus_NC_028560
Priodontes_maximus_NC_028573
Tolypeutes_tricinctus_NC_028576
Tolypeutes_matacus_NC_028575
Cabassous_tatouay_NC_028558
Cabassous_chacoensis_NC_028557
Cabassous_centralis_NC_028556
Cabassous_unicinctus_NC_028559
Cyclopes_didactylus_NC_028564
Myrmecophaga_tridactyla_NC_028572
Tamandua_tetradactyla_NC_004032
Tamandua_mexicana_NC_028574
Acratocnus_ye_Lib58
Parocnus_serus_Lib54
Choloepus_didactylus_NC_006924
Choloepus_hoffmanni_NC_027964
Mylodon_darwinii_NC_037941
Mylodon_darwinii_Lib67
Mylodon_listai_Lib16
Megatherium_sp_LibEmil
Megatheriidae_undet_LibX23
Megatheriidae_undet_LibX18
Megatheriidae_undet_Lib_X25
Nothrotheriops_shastensis_LibX32
Megalonyx_jeffersonii_Lib69
Bradypus_torquatus_NC_028555
Bradypus_pygmaeus_NC_028554
Bradypus_variegatus_NC_028501
Bradypus_tridactylus_NC_037527
0.3

Figure S1. Maximum likelihood mitogenomic tree inferred under the best-fitting partitioned model using RAxML. Related to Figure 2. Maximum-likelihood bootstrap percentages are indicating at nodes (100 replicates). Tree is rooted on midpoint. Scale is in mean number of substitutions per site.

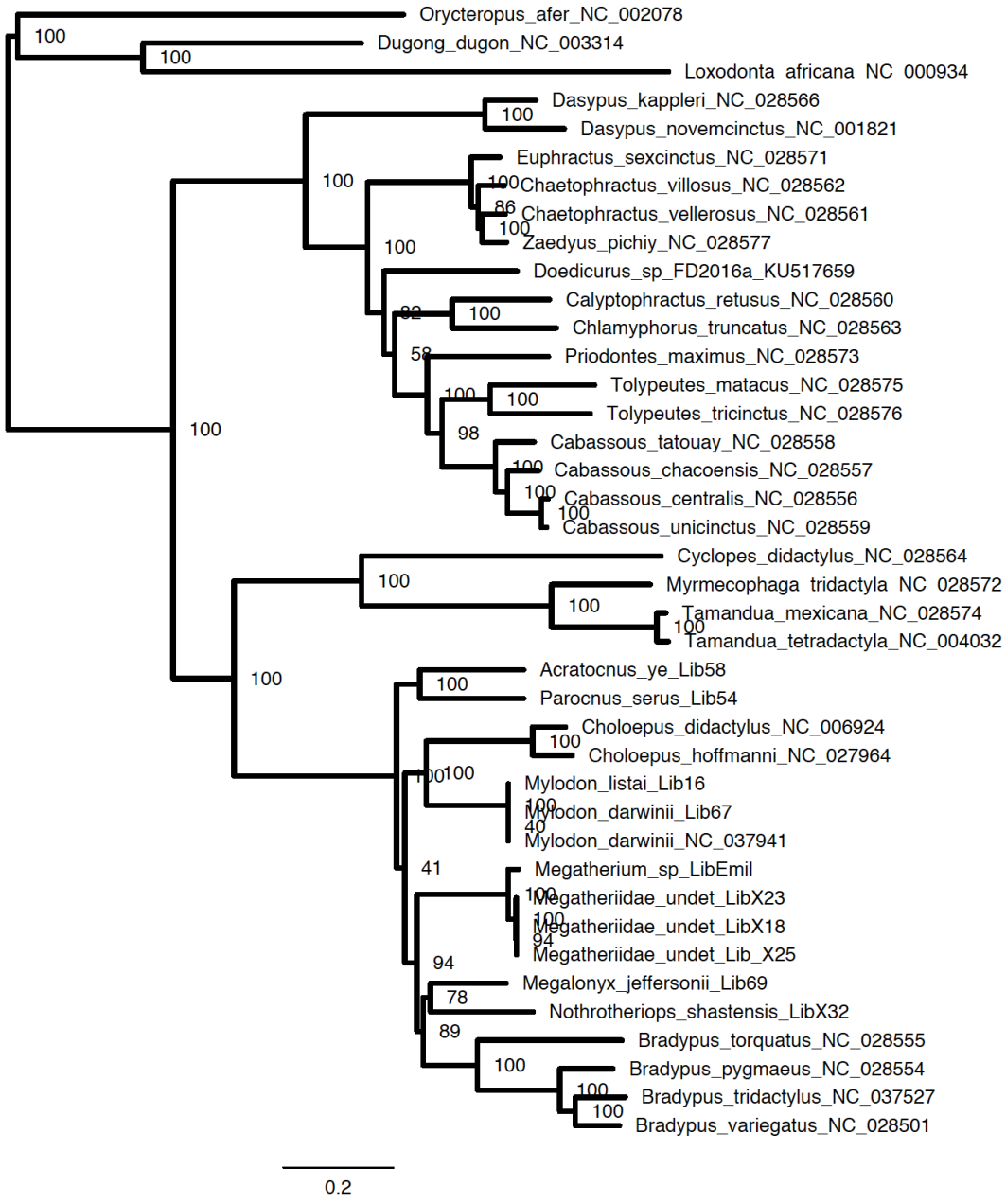
Orycteropus_afer_NC_002078
Dugong_dugon_NC_003314
Loxodonta_africana_NC_000934
Dasypus_kappleri_NC_028566
Dasypus_novemcinctus_NC_001821
Euphractus_sexcinctus_NC_028571
Chaetophractus_villosus_NC_028562
Chaetophractus_vellerosus_NC_028561
Zaedyus_pichiy_NC_028577
Doedicurus_sp_FD2016a_KU517659
Calyptophractus_retusus_NC_028560
Chlamyphorus_truncatus_NC_028563
Priodontes_maximus_NC_028573
Tolypeutes_matacus_NC_028575
Tolypeutes_tricinctus_NC_028576
Cabassous_tatouay_NC_028558
Cabassous_chacoensis_NC_028557
Cabassous_centralis_NC_028556
Cabassous_unicinctus_NC_028559
Cyclopes_didactylus_NC_028564
Myrmecophaga_tridactyla_NC_028572
Tamandua_mexicana_NC_028574
Tamandua_tetradactyla_NC_004032
Acratocnus_ye_Lib58
Parocnus_serus_Lib54
Choloepus_didactylus_NC_006924
Choloepus_hoffmanni_NC_027964
Mylodon_listai_Lib16
Mylodon_darwinii_Lib67
Mylodon_darwinii_NC_037941
Megatherium_sp_LibEmil
Megatheriidae_undet_LibX23
Megatheriidae_undet_LibX18
Megatheriidae_undet_Lib_X25
Megalonyx_jeffersonii_Lib69
Nothrotheriops_shastensis_LibX32
Bradypus_torquatus_NC_028555
Bradypus_pygmaeus_NC_028554
Bradypus_tridactylus_NC_037527
Bradypus_variegatus_NC_028501
0.2

Figure S2. Maximum likelihood mitogenomic tree inferred under the best-fitting partitioned model using IQ-TREE. Related to Figure 2. Maximum-likelihood bootstrap percentages are indicating at nodes (100 replicates). Tree is rooted on midpoint. Scale is in mean number of substitutions per site.

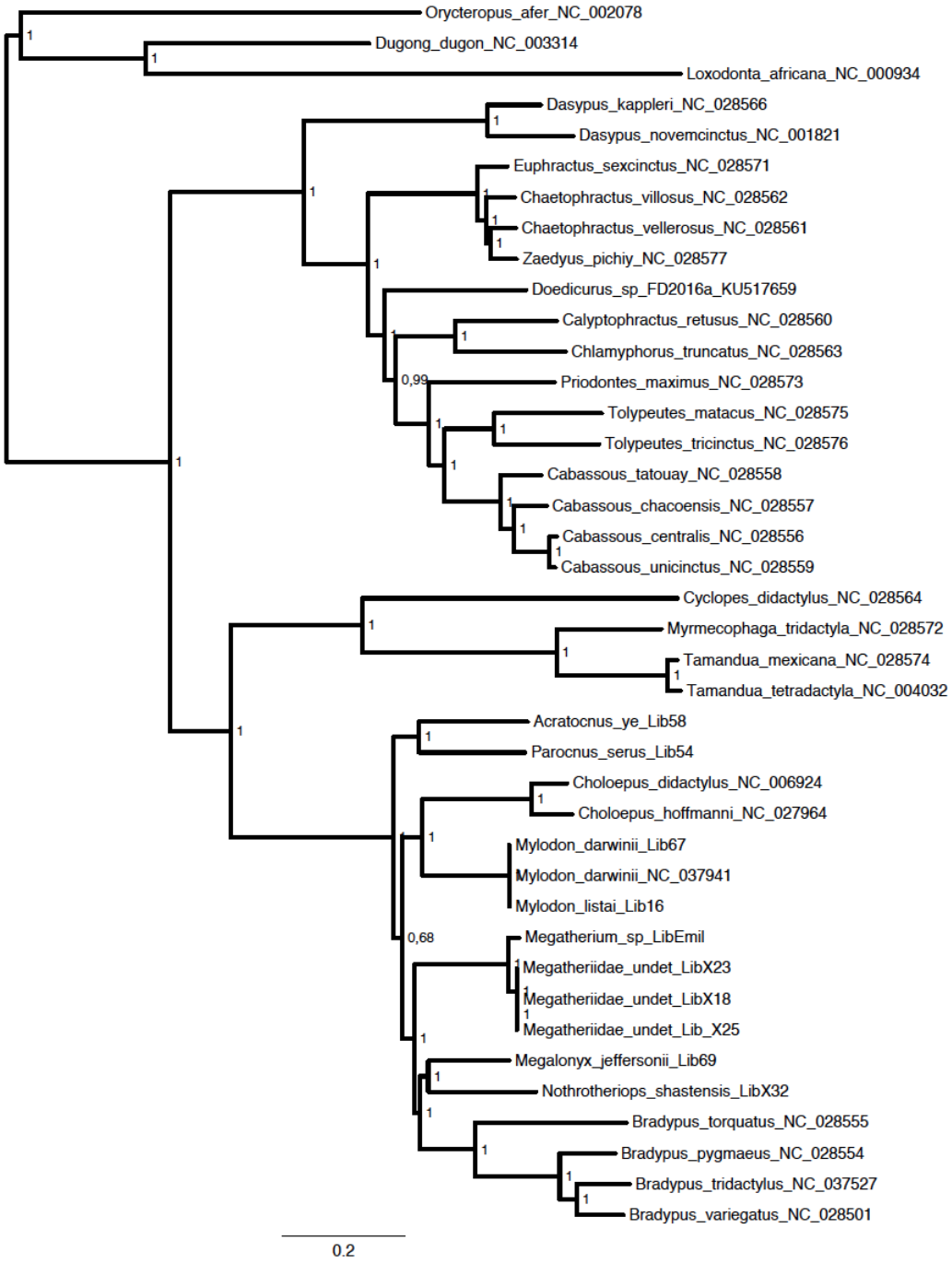
Orycteropus_afer_NC_002078
Dugong_dugon_NC_003314
Loxodonta_africana_NC_000934
Dasypus_kappleri_NC_028566
Dasypus_novemcinctus_NC_001821
Euphractus_sexcinctus_NC_028571
Chaetophractus_villosus_NC_028562
Chaetophractus_vellerosus_NC_028561
Zaedyus_pichiy_NC_028577
Doedicurus_sp_FD2016a_KU517659
Calyptophractus_retusus_NC_028560
Chlamyphorus_truncatus_NC_028563
Priodontes_maximus_NC_028573
Tolypeutes_matacus_NC_028575
Tolypeutes_tricinctus_NC_028576
Cabassous_tatouay_NC_028558
Cabassous_chacoensis_NC_028557
Cabassous_centralis_NC_028556
Cabassous_unicinctus_NC_028559
Cyclopes_didactylus_NC_028564
Myrmecophaga_tridactyla_NC_028572
Tamandua_mexicana_NC_028574
Tamandua_tetradactyla_NC_004032
Acratocnus_ye_Lib58
Parocnus_serus_Lib54
Choloepus_didactylus_NC_006924
Choloepus_hoffmanni_NC_027964
Mylodon_darwinii_Lib67
Mylodon_darwinii_NC_037941
Mylodon_listai_Lib16
Megatherium_sp_LibEmil
Megatheriidae_undet_LibX23
Megatheriidae_undet_LibX18
Megatheriidae_undet_Lib_X25
Megalonyx_jeffersonii_Lib69
Nothrotheriops_shastensis_LibX32
Bradypus_torquatus_NC_028555
Bradypus_pygmaeus_NC_028554
Bradypus_tridactylus_NC_037527
Bradypus_variegatus_NC_028501
0,99
0,68
0.2

Figure S3. Bayesian consensus mitogenomic tree inferred under the best-fitting partitioned model using MrBayes. Related to Figure 2. Clade posterior probabilities (PP) are indicated at nodes. Tree is rooted on midpoint. Scale is in mean number of substitutions per site.

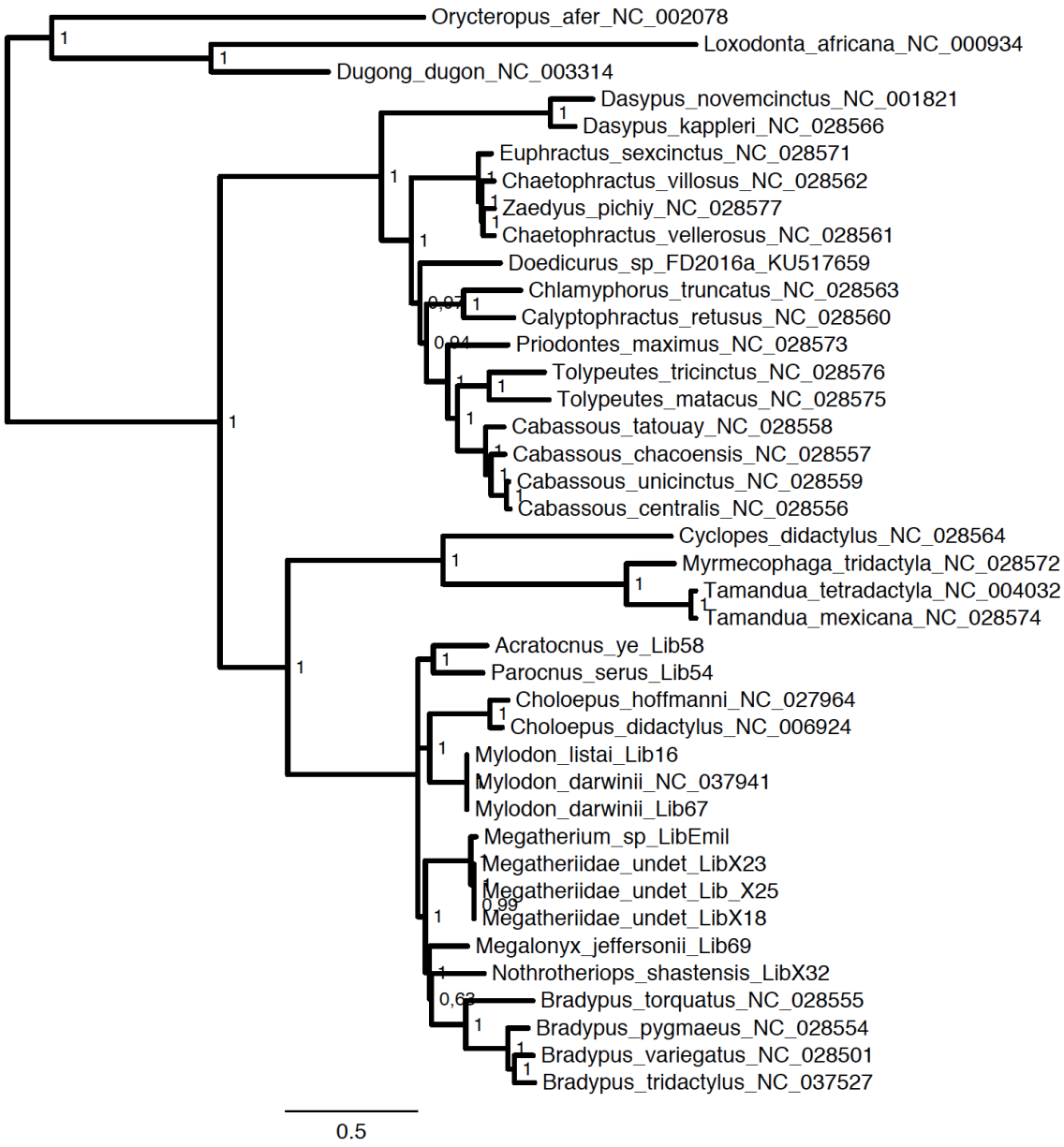
Orycteropus_afer_NC_002078
Loxodonta_africana_NC_000934
Dugong_dugon_NC_003314
Dasypus_novemcinctus_NC_001821
Dasypus_kappleri_NC_028566
Euphractus_sexcinctus_NC_028571
Chaetophractus_villosus_NC_028562
Zaedyus_pichiy_NC_028577
Chaetophractus_vellerosus_NC_028561
Doedicurus_sp_FD2016a_KU517659
Chlamyphorus_truncatus_NC_028563
Calyptophractus_retusus_NC_028560
Priodontes_maximus_NC_028573
Tolypeutes_tricinctus_NC_028576
Tolypeutes_matacus_NC_028575
Cabassous_tatouay_NC_028558
Cabassous_chacoensis_NC_028557
Cabassous_unicinctus_NC_028559
Cabassous_centralis_NC_028556
Cyclopes_didactylus_NC_028564
Myrmecophaga_tridactyla_NC_028572
Tamandua_tetradactyla_NC_004032
Tamandua_mexicana_NC_028574
Acratocnus_ye_Lib58
Parocnus_serus_Lib54
Choloepus_hoffmanni_NC_027964
Choloepus_didactylus_NC_006924
Mylodon_listai_Lib16
Mylodon_darwinii_NC_037941
Mylodon_darwinii_Lib67
Megatherium_sp_LibEmil
Megatheriidae_undet_LibX23
Megatheriidae_undet_Lib_X25
Megatheriidae_undet_LibX18
Megalonyx_jeffersonii_Lib69
Nothrotheriops_shastensis_LibX32
Bradypus_torquatus_NC_028555
Bradypus_pygmaeus_NC_028554
Bradypus_variegatus_NC_028501
Bradypus_tridactylus_NC_037527
0.5

Figure S4. Bayesian consensus mitogenomic tree inferred under the CAT-GTR+G_4 mixture model using PhyloBayes. Related to Figure 2. Clade posterior probabilities (PP) are indicated at nodes. Tree is rooted on midpoint. Scale is in mean number of substitutions per site.

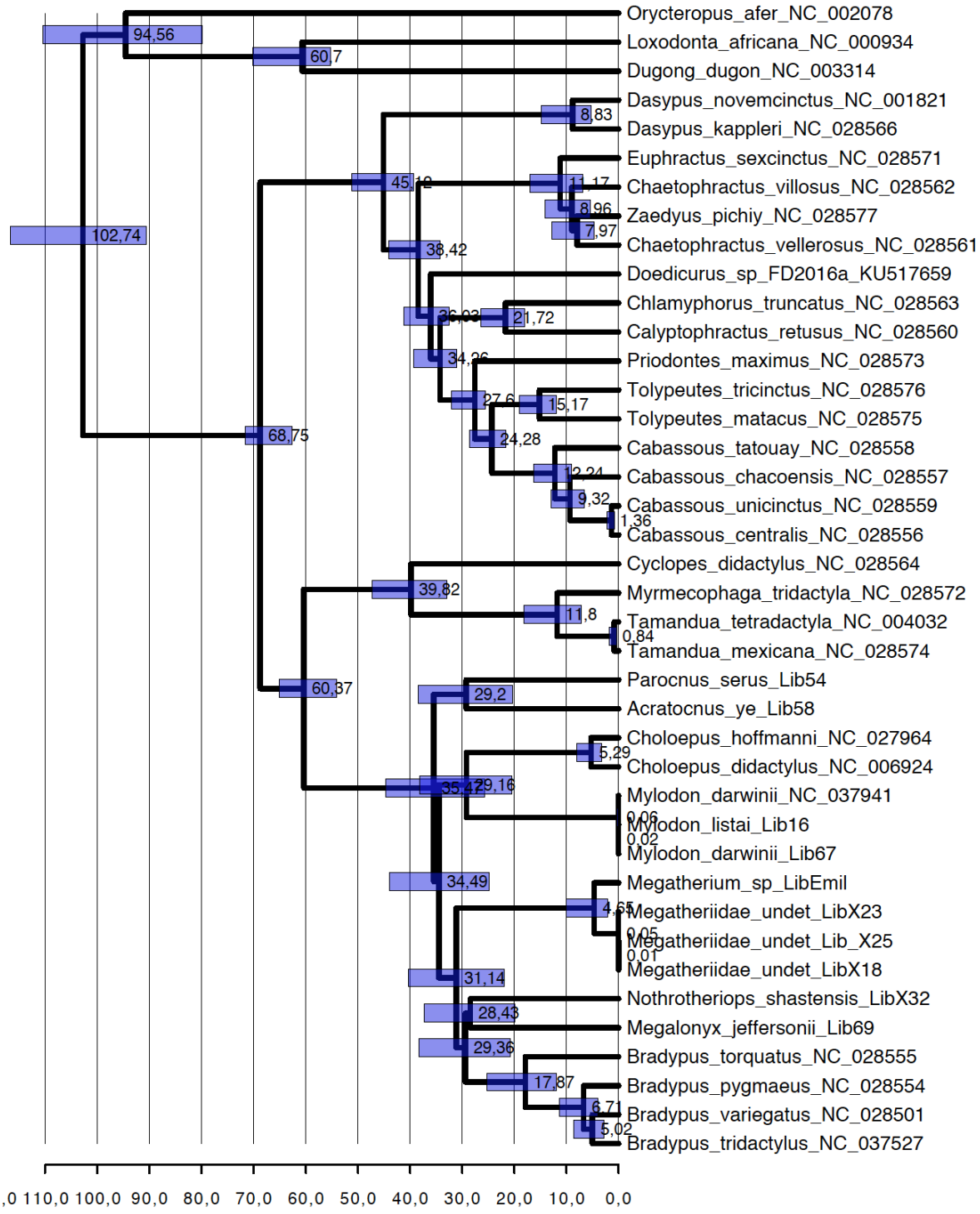
Orycteropus_afer_NC_002078
Loxodonta_africana_NC_000934
Dugong_dugon_NC_003314
Dasypus_novemcinctus_NC_001821
Dasypus_kappleri_NC_028566
Euphractus_sexcinctus_NC_028571
Chaetophractus_villosus_NC_028562
Zaedyus_pichiy_NC_028577
Chaetophractus_vellerosus_NC_028561
Doedicurus_sp_FD2016a_KU517659
Chlamyphorus_truncatus_NC_028563
Calyptophractus_retusus_NC_028560
Priodontes_maximus_NC_028573
Tolypeutes_tricinctus_NC_028576
Tolypeutes_matacus_NC_028575
Cabassous_tatouay_NC_028558
Cabassous_chacoensis_NC_028557
Cabassous_unicinctus_NC_028559
Cabassous_centralis_NC_028556
Cyclopes_didactylus_NC_028564
Myrmecophaga_tridactyla_NC_028572
Tamandua_tetradactyla_NC_004032
Tamandua_mexicana_NC_028574
Parocnus_serus_Lib54
Acratocnus_ye_Lib58
Choloepus_hoffmanni_NC_027964
Choloepus_didactylus_NC_006924
Mylodon_darwinii_NC_037941
Mylodon_listai_Lib16
Mylodon_darwinii_Lib67
Megatherium_sp_LibEmil
Megatheriidae_undet_LibX23
Megatheriidae_undet_Lib_X25
Megatheriidae_undet_LibX18
Nothrotheriops_shastensis_LibX32
Megalonyx_jeffersonii_Lib69
Bradypus_torquatus_NC_028555
Bradypus_pygmaeus_NC_028554
Bradypus_variegatus_NC_028501
Bradypus_tridactylus_NC_037527
94,56
60,7
8,83
45,19
11,17
8,96
7,97
102,74
38,42
21,72
34,26
27,6
15,17
68,75
24,28
12,24
9,32
1,36
39,82
11,8
0,84
60,37
29,2
5,29
35,42
29,16
0,06
0,02
34,49
4,65
0,05
0,01
31,14
28,43
29,36
17,87
6,71
5,02
,0 110,0 100,0 90,0 80,0 70,0 60,0 50,0 40,0 30,0 20,0 10,0 0,0

Figure S5. Bayesian mitogenomic chronogram. Related to Figure 3. This chronogram was inferred under the CAT-GTR+G_4 mixture model and an autocorrelated lognormal model of clock relaxation using PhyloBayes. Time scale is in million years.

Subset	Best Model	# Sites	Subset Partitions
1	GTR+I+G	7,875	12S, 16S, tRNAs, ND5_p1, CYTB_p1, ATP6_p1, ND1_p1, ND3_p1, ND4L_p1, ND4_p1, ND2_p1, ATP8_p3, ATP8_p2, ATP8_p1, COX1_p1, COX3_p1, COX2_p1, ND6_p1, ND6_p2
2	GTR+I+G	3,554	COX1_p2, COX2_p2, COX3_p2, CYTB_p2, ND1_p2, ATP6_p2, ND4_p2, ND5_p2, ND2_p2, ND4L_p2, ND3_p2
3	GTR+I+G	3,554	CYTB_p3, ND2_p3, ND1_p3, ND5_p3, COX1_p3, ND4_p3, ND3_p3, ND4L_p3, ATP6_p3, COX2_p3, COX3_p3
4	GTR+I+G	174	ND6_p3

***** Settings: A priori partitions (42), Branch lengths (Unlinked), Models (GTR+G, GTR+I+G), Model selection (BIC), Search (Greedy).

Table S1. Detailed results of the PartitionFinder analysis for RAxML. Related to Figure 2.

Subset	Best Model	# Sites	Subset Partitions
1	GTR+F+I+G4	2,710	12S, 16S, CYTB_p1
2	GTR+F+I+G4	1,218	ATP6_p1, ND1_p1, ND3_p1, ND4L_p1, ND4_p1
3	TVM+F+I+G4	2,552	ATP6_p2, CYTB_p2, ND1_p2, ND2_p2, ND3_p2, ND4L_p2, ND4_p2, ND5_p2
4	TIM3+F+I+G4	968	ATP6_p3, COX1_p3, COX2_p3
5	TN+F+I+G4	198	ATP8_p1, ATP8_p2, ATP8_p3
6	TIM2e+I+G4	513	COX1_p1
7	TPM2+F+I+G4	1,002	COX1_p2, COX2_p2, COX3_p2
8	TIM2e+I+G4	489	COX2_p1, COX3_p1
9	TIM3+F+I+G4	2,586	COX3_p3, CYTB_p3, ND1_p3, ND2_p3, ND3_p3, ND4L_p3, ND4_p3, ND5_p3
10	TVM+F+I+G4	954	ND2_p1, ND5_p1
11	TN+F+I+G4	174	ND6_p1
12	TVM+F+G4	174	ND6_p2
13	TIM2+F+I+G4	174	ND6_p3
14	GTR+F+I+G4	1,445	tRNAs

* Settings: A priori partitions (42), Branch lengths (Unlinked), Models (All), Model selection (BIC), Search (Greedy).

Table S2. Detailed results of the ModelFinder analysis for IQ-TREE. Related to Figure 2.

Subset	Best Model	# Sites	Subset Partitions
1	GTR+I+G	7,743	12S, 16S, tRNAs, ATP8_p1, ND2_p1, ATP6_p1, ND3_p1, ND1_p1, ND5_p1, CYTB_p1, ND4L_p1, ND4_p1, COX1_p1, COX2_p1, COX3_p1, ND6_p1, ND6_p2
2	GTR+I+G	3,620	COX1_p2, COX2_p2, ATP8_p2, ND5_p2, ND2_p2, ATP6_p2, ND4_p2, ND3_p2, ND1_p2, COX3_p2, CYTB_p2, ND4L_p2
3	GTR+I+G	3,620	COX3_p3, ND4_p3, ND3_p3, ND4L_p3, CYTB_p3, ND2_p3, ND5_p3, ND1_p3, ATP8_p3, COX2_p3, ATP6_p3, COX1_p3
4	GTR+I+G	174	ND6_p3

***** Settings: A priori partitions (42), Branch lengths (Unlinked), Models (JC, K80, SYM, F81, HKY, GTR, JC+G, K80+G, SYM+G, F81+G, HKY+G, GTR+G, JC+I, K80+I, SYM+I, F81+I, HKY+I, GTR+I, JC+I+G, K80+I+G, SYM+I+G, F81+I+G, HKY+I+G, GTR+I+G), Model selection (BIC), Search (Greedy).

Table S3. Detailed results of the PartitionFinder analysis for MrBayes. Related to Figure 2.